HEAT TRANSFER ANALYSIS OF A
ROTATING HEAT PIPE CONTAINING
INTERNAL, AXIAL FINS

Robert David Corley

NAVAL POSTGRADUATE SCHOOL
Monterey, California

THESIS

HEAT TRANSFER ANALYSIS OF A
ROTATING HEAT PIPE CONTAINING
INTERNAL, AXIAL FINS

by

Robert David Corley

June 1976

Thesis Advisor: P. J. Marto

Approved for public release; distribution unlimited.

REPORT DOCUMENTATION PAGE		READ INSTRUCTIONS BEFORE COMPLETING FORM
1. REPORT NUMBER	2. GOVT ACCESSION NO.	3. RECIPIENT'S CATALOG NUMBER
4. TITLE (and Subtitle) Heat Transfer Analysis of a Rotating Heat Pipe Containing Internal, Axial Fins		5. TYPE OF REPORT & PERIOD COVERED Master's Thesis: June 1976
		6. PERFORMING ORG. REPORT NUMBER
7. AUTHOR(s) Robert David Corley		8. CONTRACT OR GRANT NUMBER(s)
9. PERFORMING ORGANIZATION NAME AND ADDRESS Naval Postgraduate School Monterey, California 93940		10. PROGRAM ELEMENT, PROJECT, TASK AREA & WORK UNIT NUMBERS
11. CONTROLLING OFFICE NAME AND ADDRESS Naval Postgraduate School Monterey, California 93940		12. REPORT DATE June 1976
		13. NUMBER OF PAGES
14. MONITORING AGENCY NAME & ADDRESS(if different from Controlling Office) Naval Postgraduate School Monterey, California 93940		15. SECURITY CLASS. (of this report) Unclassified
		15a. DECLASSIFICATION/DOWNGRADING SCHEDULE

16. DISTRIBUTION STATEMENT (of this Report)

Approved for public release; distribution unlimited.

17. DISTRIBUTION STATEMENT (of the abstract entered in Block 20, if different from Report)

18. SUPPLEMENTARY NOTES

19. KEY WORDS (Continue on reverse side if necessary and identify by block number)

Film Condensation
Heat Pipe
Finite Elements
Fins

20. ABSTRACT (Continue on reverse side if necessary and identify by block number)

An analytical study was undertaken to determine the two-dimensional wall conduction effects in an internally finned, rotating heat pipe. The finite element method was employed to generate computer results for a copper condenser with triangular fins. Heat transfer rates were shown to be approximately seventy-five percent greater than that predicted by an earlier, one-dimensional analysis. Heat transfer rates were

found to be insensitive to rotational speed and fin half-angle.
Due to numerical difficulties within the finite element program,
no data was obtained for the finned, stainless steel condenser.

Heat Transfer Analysis of a
Rotating Heat Pipe Containing
Internal, Axial Fins

by

Robert David Corley
Ensign, United States Navy
B.S.A.E., United States Naval Academy, 1975

Submitted in partial fulfillment of the
requirements for the degree of

MASTER OF SCIENCE IN MECHANICAL ENGINEERING

from the

NAVAL POSTGRADUATE SCHOOL
June 1976

ABSTRACT

An analytical study was undertaken to determine the
two-dimensional wall conduction effects in an internally
finned, rotating heat pipe. The finite element method was
employed to generate computer results for a copper condenser
with triangular fins. Heat transfer rates were shown to be
approximately seventy-five percent greater than that pre-
dicted by an earlier, one-dimensional analysis. Heat transfer
rates were found to be insensitive to rotational speed and
fin half-angle. Due to numerical difficulties within the
finite element program, no data was obtained for the finned,
stainless steel condenser.

TABLE OF CONTENTS

TABLE OF SYMBOLS

a_1 Constant multiplier of second degree term of parabolic temperature distribution equation, $°F/ft^2$

b_1 Constant multiplier of first degree term of parabolic temperature distribution equation, $°F/ft$

b Fin height, ft

h_{avg} Average nodal convective coefficient, $Btu/hr-ft^2-°F$

h_{out} External environment convective coefficient, $Btu/hr-ft^2-°F$

h_{fg} Latent heat of vaporization of working fluid, Btu/lbm

k_f Fluid thermal conductivity, $Btu/hr-ft-°F$

k_w Condenser wall material thermal conductivity, $Btu/hr-ft-°F$

ℓ Direction cosine of outer normal to a boundary's surface, dimensionless

$\dot{M}_1$ Fin condensate mass flow rate per unit condenser length, $lbm/hr-ft$

$\dot{M}_{tot}$ Total condensate mass flow rate per unit condenser length, $lbm/hr-ft$

N Finite element shape function, dimensionless

N_{fin} Number of fins around the condenser circumference, dimensionless

$\dot{Q}_1$ Fin condensate heat transfer rate per unit condenser length, $Btu/hr-ft$

$\dot{Q}_2$ Trough condensate heat transfer rate per unit condenser length, $Btu/hr-ft$

$\dot{Q}_i$ Incremental heat transfer rate per unit condenser length, $Btu/hr-ft$

$\dot{Q}_{tot}$ Total condenser heat transfer rate, Btu/hr

R_2 Average condenser wall radius at endplate, ft

T_S Fluid saturation temperature, °F

T_W Condenser inner wall surface temperature, °F

T_∞ External environment temperature, °F

t Condenser wall thickness, ft

t^* Effective condenser wall thickness, ft

w Fin condensate velocity in the z-direction, ft/hr

$\bar{w}$ Fin condensate velocity in the z-direction averaged over film thickness, ft/hr

x Coordinate measuring distance along apex of fin

y Coordinate measuring perpendicular distance from fin surface

z Coordinate measuring distance along fin surface from apex of fin

Greek

α Fin half-angle, degrees

β Constant multiplier of first degree term in linear temperature distribution equation, °F/ft

δ Fin condensate thickness, ft

δ^* Trough condensate thickness, ft

ε Local trough width, ft

ε_0 Fin base width, ft

ϕ Condenser cone half-angle, degrees

ρ_f Density of working fluid, lbm/ft³

τ Shear stress, lbf/ft²

μ_f Viscosity of working fluid, lbm/ft-hr

ω Rotation rate, radians/hr

Other Symbols

⟨ ⟩   Row matrix

{ }   Vector matrix

Subscripts

avg   refers to average condition

b   refers to specified boundary only

f   refers to fluid condition

i   refers to increment value

j   refers to iterate value

out   refers to outside environment condition

s   refers to saturated condition

tot   refers to total value

w   refers to value along wall

∞   refers to outside environment condition

ACKNOWLEDGEMENTS

The author wishes to offer his deepest thanks to
Dr. P. J. Marto of the Naval Postgraduate School for his
advice and encouragement throughout the course of this thesis
work.   Thanks are also extended to Dr. D. Salinas for his
assistance with the finite element section of the study.

I. INTRODUCTION

A. THE ROTATING, NON-CAPILLARY HEAT PIPE

The rotating, non-capillary heat pipe is a self-contained
device designed to transfer large quantities of heat in a
rotating system. The heat pipe contains an evaporator, a
condenser, and a working fluid as shown in Figure 1. The
working fluid is vaporized by heat addition at the evaporator.
The vapor flows toward the condenser end as a result of a
vapor pressure differential. There, the vapor condenses on
the inner wall, releasing its latent heat of vaporization.
The condensate then returns to the evaporator where the cycle
is repeated.

The difference between the conventional heat pipe and the
rotating, non-capillary heat pipe is the condensate return
mechanism. A conventional heat pipe employs the capillary
pumping action of an internal porous wick to transport the
condensate to the evaporator. The disadvantage of this scheme
is the resistance to condensate flow through the wick. Addi-
tionally, the presence of nucleate boiling in the evaporator
could create bubbles inside the wick structure, reducing the
effectiveness of the pumping action [1][1]. In the rotating
heat pipe, rotation about its longitudinal axis establishes
a centrifugal force field which, when combined with a slight

---

[1] Numbers in brackets indicate references listed in the
Bibliography.

10

taper of the condenser section, forces the condensate toward the evaporator. At high rotation rates, the heat transfer rate is significantly increased over the rate achieved in conventional heat pipes of similar dimensions.

B. BACKGROUND

Previous analyses [2-9] of the rotating heat pipe have been conducted to determine its performance characteristics. These studies determined, among other things, that under normal circumstances, the heat transfer rate is limited primarily by the amount of heat which can be transferred through the condenser wall.

In an effort to improve the condenser heat transfer performance, Schafer [8] estimated and compared the thermal resistances across the condensate film, the wall, and the outside convective film using Woodard's earlier data [9]. He showed that with the use of outside spray cooling and a thin copper wall, the controlling resistance is the inside film resistance. Schafer suggested that this resistance can be reduced (1) by the proper selection of working fluid, and (2) through the use of internal axial fins as sketched in Figure 2a.

Machining axial fins into the inner surface of the condenser would improve heat transfer performance through two mechanisms: a decrease in condensate film thickness near the apex of each fin, and an increase in inner wall surface area. However, with the addition of fins, the wall thermal

resistance would also increase due to the increase in
effective wall thickness. Of course, the use of copper as
the wall material, because of its high thermal conductivity,
would minimize the added wall resistance.

Schafer then developed an analytical model of the intern-
ally finned condenser for the case of fins of triangular
profile (Figures 2a, 2b). In the analysis, he assumed one-
dimensional heat conduction through the wall and assumed a
linearly decreasing temperature profile from the fin apex
(point A) to the midpoint of the trough (point C). Results
from the analysis indicated significantly improved heat
transfer rates for the finned condenser compared to the smooth
condenser. He pointed out, however, that two-dimensional
conduction effects may be significant so that a more detailed
analysis of the heat conduction problem within the wall was
necessary.

C. OBJECTIVES

The objectives of this study were, therefore, to (1)
develop an analytical solution to account for two-dimensional
conduction effects within the wall for the triangular fin
profile, and (2) compare this solution with the solution
derived by Schafer.

12

II. THEORETICAL PROGRAM

A. REVIEW OF SCHAFER ANALYSIS [8]

Schafer's study considered an internal fin geometry represented by Figure 2a. Since the sum of wall thickness and fin height was assumed to be much smaller than condenser radius, an average radius from any point on the axis to the condenser wall was taken to be the distance from the axis to a position midway between the base of the fin and the apex of the fin, r_1. The centrifugal acceleration term was then evaluated at this average radius, $r_1 \omega^2$.

The thin wall assumption also allowed the curvature of the wall to be neglected. The problem could then be analyzed using a planar conduction heat transfer model as shown in Figure 2b. Furthermore, because of repetitive geometry the problem could be reduced to the simpler geometry shown in Figure 3. Cartesian coordinates were then selected, as shown, to permit a simplified fin condensation analysis.

Assumptions in the analysis were based upon the earlier work of Ballback [2]. These assumptions were similar to those used in the Nusselt analysis of film condensation on a wall. The more important of these assumptions are:

   (1) steady state operation,

   (2) film condensation, as opposed to dropwise condensation,

   (3) laminar condensate flow along both the fin and the trough,

   (4) static balance of forces within the condensate,

13

(5) one-dimensional conduction heat transfer through the film thickness (no convective heat transfer),

(6) no liquid-vapor interfacial shear stresses, and

(7) no condensate subcooling.

Additional assumptions in the analysis are noted later.

The complete development of Schafer's finned condenser heat transfer theory is presented in his thesis [8]. However, since the fluid flow and heat transfer theory was applicable to the two-dimensional conduction heat transfer analysis, a summary of his work is presented here, prior to the development of the two-dimensional conduction model.

1. Fin Condensate Mass Flow

A Nusselt analysis was performed for film condensation on the wall of the fin. In this analysis, the fluid momentum equation was constructed to account for the effects of condenser cone half-angle, ϕ, fin half-angle, α, and the centrifugal force field. The pressure differential term was neglected. Condensate flow on the fin was assumed to be in the z-direction only.

An expression for fluid velocity, $w(y,z)$, was then derived by substituting the shear stress equation for laminar flow, $\tau_z = \mu_f \frac{\partial w}{\partial y}$, into the momentum equation and solving for $w(y,z)$. Average velocity, $\overline{w}(z)$, was then found by integrating $w(y,z)$ over y from $y = 0$ to $y = \delta(z)$, the local film thickness. This average velocity was then placed in the fin mass flow equation to yield an expression for fluid mass flow rate along the fin per unit condenser length as a function of $\delta(z)$,

14

$$\dot{M}_1(z) = \frac{\rho_f^2 \omega^2 (R_2 + x \sin \phi) \cos \phi \cos \alpha \, \delta^3(z)}{3\mu_f} . \qquad (1)$$

2. Trough Condensate Mass Flow Equation

Fluid flow within the trough was assumed to be one-dimensional in the x-direction and of constant velocity across the width of the trough. Therefore, condensate flowing from the fins into the trough was assumed to accelerate immediately to the velocity of the trough fluid. Cross-sectional area of the trough condensate region was twice the area shown in Figure 4.

The x-direction momentum equation for an infinitesimal fluid element in the trough was constructed with the pressure differential term neglected. The trough mass flow expression was then developed in a manner similar to the development of the fin mass flow equation (1). The average trough velocity was derived and substituted into the trough mass flow equation to yield total mass flow through the trough region,

$$\dot{M}_{tot}(x) = \frac{\rho_f^2 \omega^2 (R_2 + x \sin \phi) \delta^{*2}(x) \sin \phi}{3\mu_f}$$

$$(\epsilon \delta^*(x) + \sin \alpha \cos \alpha \, \delta^{*2}(x)), \qquad (2)$$

where the expression in the second parenthesis is the cross-sectional area of the trough condensate region.

Total condensate mass flow was identical to trough condensate mass flow since all condensate eventually flowed to the trough. Therefore, once the total mass flow rate at

15

any position x was known, trough condensate thickness, $\delta^*(x)$, could be determined using equation (2).

3.   Condenser Heat Transfer Determination

Schafer assumed zero heat flux boundary conditions on both sides of the wall section shown in Figure 4. Temperature at the fin apex was taken to be fluid saturation temperature since film thickness at this position was assumed to be zero.

He then imposed a linearly decreasing temperature on the inner wall surface from the apex of the fin to the mid-channel position. The surface temperature expression became

$$T_s - T_w(z) = \beta z, \tag{3}$$

where β was an unknown constant. This choice of temperature distribution was arbitrary but allowed a simplified one-dimensional conduction analysis of the condenser wall. He then imposed the restriction that no heat transfer would occur through section BE of the wall (Figure 3). All heat transfer through the fin surface, thus, flowed out of the wall through section FE.

Heat transfer through the fin was equated with one-dimensional heat transfer through a rectangular geometry of the same width as section FE, and of height, t^*, equal to t plus one-half the fin height (Figure 4). Temperature of the upper surface of the rectangle was set equal to the tempera-ture at a point midway between positions A and B. The expression for heat transfer rate per unit condenser length through the wall and outer convective thermal resistance

of the fin became

$$\dot{Q}_1(z^*) = \frac{[(T_s - \frac{\beta z_0}{2}) - T_\infty]}{(\frac{t^*}{k_w} + \frac{1}{h_{out}})} \frac{\varepsilon_0}{2} . \tag{4}$$

It was then desired to develop an expression for $\dot{Q}_1(z^*)$ in terms of the heat transfer rate through the fin condensate film. First, the equation for fin condensate film thickness was derived by differentiating (1) with respect to z and substituting the result into the differentiated equation for mass flow rate per unit condenser length,

$$d\dot{M}_1(z) = \frac{d\dot{Q}_1(z)}{h_{fg}} = \frac{1}{h_{fg}} [k_f (\frac{T_s - T_w(z)}{\delta(z)})] dz . \tag{5}$$

The expression produced was algebraically rearranged to form a differential equation in $\delta(z)$,

$$\delta^3(z)d\delta(z) = \frac{k_f (T_s - T_w(z)) \mu_f dz}{\rho_f^2 \omega^2 (R_2 + x \sin \phi) h_{fg} \cos \phi \cos \alpha} . \tag{6}$$

Equation (3) was then substituted in (6) and the result integrated over z from z = 0 to z to give an equation for $\delta(z)$,

$$\delta(z) = [\frac{2 k_f \beta \mu_f}{\rho_f^2 \omega^2 (R_2 + x \sin \phi) h_{fg} \cos \phi \cos \alpha}]^{1/4} z^{1/2} . \tag{7}$$

The value for fin heat transfer rate per unit condenser length was then evaluated using

$$\dot{Q}_1(z^*) = h_{fg} \dot{M}_1(z^*) \tag{8}$$

17

where z^* is defined in Figure 4. This expression was set
equal to (4) to yield a transcendental equation in β,

$$\frac{[(T_s - \frac{\beta z_0}{2} - T_\infty]}{(\frac{t^*}{k_w} + \frac{1}{h_{out}})} \frac{\varepsilon_0}{2}$$

$$= \frac{(2K_f\beta)^{3/4} (\rho_f\omega)^{1/2} [(R_2 + x\sin\phi) h_{fg} \cos\phi \cos\alpha]^{1/4} z^{*3/2}}{3\mu_f^{1/4}},$$

(9)

where ε_0 was the width of the base of the fin. The expressions
on the left and right hand sides of this equation were equiva-
lent only when all boundary conditions were satisfied. The
task was then to solve iteratively for β until equation (9)
was satisfied. $\dot{Q}_1(z^*)$ was then determined in equation (4)
using the final iterated value of β.

Heat transfer rate from the trough region was evaluated
using

$$\dot{Q}_2(x) = k_f \frac{(T_s - T_{avg})}{\delta^*(x)} \frac{\varepsilon}{2},$$

(10)

where T_{avg} was calculated as an average temperature of the
trough wall and ε was the total trough width (Figure 4).

A flowchart description of the computer program used
in the Schafer analysis is given in Figure 5. The axial
length of the condenser was first divided into increments
of equal length, Δx. Solution of the heat transfer problem
was then started by assuming an initial trough condensate
thickness, $\delta^*_1 = 0.00006752$ feet. This initial value was
based upon a mass flow analysis by Sparrow and Gregg of
condensation on a rotating disk [10]. It was assumed in

18

Schafer's analysis that the effect on the Sparrow and Gregg
solution of enclosing the disk within the condenser would
be minimal. A study of the effects of a ten-fold increase
or decrease from the above value of δ^*_1 indicated that the
initial δ^*_1 assumption would not affect the heat transfer
solution by more than ten percent. Therefore, the deter-
mination of an exact value of initial trough condensate
thickness was not crucial to the problem.

Calculation of condensate mass flow contribution from
the endplate then followed. Then, for each increment Δx, an
initial value of β was calculated by removing the $\frac{\beta z_0}{2}$ term
from the left side of equation (9) and solving directly for
β. The full equation was then employed to solve iteratively
for β. Calculation of incremental fin heat transfer rate
then followed by multiplying the value obtained in (4) by
the incremental length, Δx. Incremental trough heat transfer
rate was next evaluated by multiplying equation (10) by Δx.
Incremental trough and fin heat transfer rates were then
summed to yield the total incremental heat transfer rate for
the geometry of Figure 4.

Total incremental mass flow rate was evaluated by
dividing twice the sum of the incremental trough and fin heat
transfer rates by the latent heat of vaporization of the fluid.
As the incrementation progressed, incremental mass flow rates
were added to mass flow from preceding increments to yield
$\dot{M}_{tot}$ (x). Equation (2) was then solved for $\delta^*(x)$ with the
aid of a polynomial rootfinder subroutine. The new value of

19

$\delta^*(x)$ was then used to begin the solution for the next increment. When the total length of the condenser had been traversed, total heat transfer rate was evaluated.

$$\dot{Q}_{tot} = 2 N_{fin} \sum_{i=1}^{100} \Delta x [\dot{Q}_1 (z^*)_i + \dot{Q}_2 (x)_i]. \qquad (11)$$

B. TWO-DIMENSIONAL HEAT TRANSFER SOLUTION

1. Introduction

In this study, two-dimensional conduction through the condenser wall was considered in the heat transfer analysis using a finite element solution. The finite element method was chosen over the method of finite differences because of considerations involving wall geometry and computer utilization time. Myers [11] has shown that when these methods are compared for the case of two-dimensional conduction in a rectangular block with heat generation, the finite element method more closely approximates the exact solution when the number of nodal points considered in each method are equal. This is particularly true when the nodal point meshes are coarse.

To achieve the same accuracy as with the finite element method, the finite difference method must use a finer nodal mesh, especially for non-rectangular geometries. Additionally, when fins of different shape are considered, the mesh of the finite difference model must be completely reconstructed for each new shape. In the finite element program, however, a simple change in nodal coordinates is all that is necessary

20

to accommodate the change in fin shape. Since future studies may analyze the use of varied fin shapes with the rotating heat pipe, it was desired to incorporate the more flexible finite element method in the computer program to avoid having to rearrange the program for each fin shape.

While the accuracy of the finite element method is superior, the finite difference method requires less computer utilization time for the same number of nodal points. If a finite difference model of finer mesh was chosen, the decrease in computer time due to the method might be offset by an increase in time required for the increased number of nodes. The overall improvement in computer utilization time might, therefore, be minimal. As a result, in this study, the choice of method was not based upon computer time requirements. Also, a finite element computer program [12] was available which could be adapted for the purposes of this analysis. For the reasons outlined above, therefore, the finite element method was selected.

The steady state differential equation for conduction heat transfer is given in Arpaci's text [13] as

$$\frac{\partial}{\partial y} \left(k_y \frac{\partial T}{\partial y} \right) + \frac{\partial}{\partial z} \left(k_z \frac{\partial T}{\partial z} \right) = 0. \tag{12}$$

Boundary conditions are normally of two kinds; those of specified temperature on a boundary,

$$T = T_b , \text{ (boundary b only)} \tag{13}$$

and those of specified heat flux or convective condition

on the boundary,

$$(k_y \frac{\partial T}{\partial y} \ell_y)_b + (k_z \frac{\partial T}{\partial z} \ell_z)_b$$

$$+ [h(T - T_\infty)]_b + q_b = 0, \text{ (boundary b only)}$$

(14)

where ℓ_y and ℓ_z are direction cosines of the outward
normal to the boundary's surface.

2. The Finite Element Method

Many references including [11], [14], and [15] develop
the concept of using material elements of finite dimensions
within a structure to model the differential equation and its
boundary conditions. The steady-state field equation, (12),
may be discretized by considering that the temperature at any
point within an element is a function of the temperatures of
specified nodes on that element,

$$T = \langle N \rangle \{ T \}^e,$$

(15)

where $\langle N \rangle$ is the row matrix shape function of position and
$\{ T \}^e$ is the nodal temperature vector for the element. The
field equation and boundary equations for each element may
be mathematically rearranged and integrated to yield a matrix
system of equations for that element,

$$[H]^e \{ T \}^e = -\{ F \}_b^e ,$$

(16)

where

$$[H]^e = \int_{s_e} k (\{\frac{\partial N}{\partial z}\} \langle \frac{\partial N}{\partial z} \rangle + \{\frac{\partial N}{\partial y}\} \langle \frac{\partial N}{\partial y} \rangle) dz \, dy ,$$

(17)

and

22

$$\{F\}_b^e = - (\int_{c_e} q \{N\} dc)_b$$

$$+ (\int_{c_e} \{N\} h \langle N \rangle dc)_b - h\{T_\infty\}_b c_b. \qquad (18)$$

Equation (18) is applied only over relevant boundaries. The element matrix equations are then assembled into a master matrix equation for the entire structure. Solution by numerical methods then follows.

The convective boundary conditions were applied in the finite element solution of the finned condenser using a lumped convective condition formulation. Average nodal convective coefficients, h_{avg}, were determined for each node subject to a convective environment. The nodal h_{avg} values were then considered to be constant over the boundary region associated with the node. The method of determination of these coefficients is described in a later section.

Equation (18) was, thus, reduced to the following form,

$$\{F\}_b^e = (\{h_{avg} T\}_b^e - \{h_{avg} T_\infty\}_b^e) c_b. \qquad (19)$$

This lumping procedure reduced the complexity of the convective condition calculations and did not seriously affect the values within the master matrix, [H].

Reference [15] presents a development of the isoparametric finite element concept. This concept allows the solution of equations (12), (13), and (14) for elements of non-uniform shape. The application of the method of finite elements is, therefore, extended to a wider range of physical problems.

23

The eight-nodal finite element mesh used in the two-dimensional analysis of the axially finned condenser is shown in Figure 6. A computer program for the case of two-dimensional conduction was developed using a modified version of the three-dimensional, isoparametric finite element program assembled by Lew [12].

3. Test Cases

Before the finite element solution was applied to the condenser problem, a series of test cases were analyzed. These cases allowed a comparison of analytical solutions to results obtained using the finite element program. The two-dimensional heat conduction problems studied were

(1) a rectangular block with specified surface temperature,

(2) a rectangular block in a uniformly convective environment,

(3) a rectangular block with a triangular fin in a uniformly convective environment,

(4) a rectangular block with a convex parabolic fin in a uniformly convective environment, and

(5) a rectangular block with a concave parabolic fin in a uniformly convective environment.

Results of the test cases are presented in Figures 7-11 with values obtained using the finite element program placed in brackets. For the first two cases, the heat transfer rates calculated with the aid of the finite element computer program agreed well with the exact, two-dimensional solutions. Although finite element heat transfer solutions were relatively accurate, nodal temperature values were slightly different from the exact values. This temperature discrepancy

24

led to numerical difficulties when the finite element solution was applied to the stainless steel condenser. These difficulties will be discussed more fully in Chapter III.

For the finned block cases, analytical expressions were derived for heat transfer rates through extended surfaces using the one-dimensional fin analysis as described in [16]. Heat transfer rates calculated by the finite element program for this uniformly convective environment did not vary significantly from the one-dimensional results. Since test case results from the finite element program agreed favorably with the derived results, the program was assumed to be operating properly and was applied to the condenser heat transfer problem.

4. Condenser Boundary Condition Application

The axially finned condenser problem was analyzed by considering the geometry of Figure 6. Boundary conditions for the problem were considered to be the same as those in the Schafer analysis with the exception of the inner surface temperature distribution. Instead of using a linearly decreasing temperature profile along the wall from the apex of the fin to the midpoint of the channel, a parabolic distribution was assumed and used to calculate average nodal convective coefficients.

The Nusselt analysis of the fin condensation problem yielded a differential equation in $\delta(z)$, fin condensate thickness, which is identical to equation (6) used in Schafer's analysis.

Consistent with the eight-nodal finite element concept, a parabolic temperature distribution was then assumed to exist along the fin surface using the boundary condition, $T = T_S$ at $z = 0$, since $\delta(0) = 0$. Therefore,

$$T_w(z) = a_1 z^2 + b_1 z + T_S , \tag{20}$$

or

$$T_S - T_w(z) = -a_1 z^2 - b_1 z , \tag{21}$$

where a_1 and b_1 were unknown constants.

When (21) was substituted into equation (6) and the result integrated from $z = 0$ to z, the expression for $\delta(z)$ became

$$\delta(z) = \left[\frac{4 k_f (- a_1 \frac{z^3}{3} - b_1 \frac{z^2}{2}) \mu_f}{\rho_f^2 \omega^2 (R_2 + x \sin \phi) h_{fg} \cos \phi \cos \alpha} \right]^{1/4} . \tag{22}$$

The local convective heat transfer coefficient, assuming one-dimensional heat conduction through the thin condensate film, was then

$$h(z)_{fin} = \frac{k_f}{\delta(z)} = \left[\frac{k_f^3 \rho_f^2 \omega^2 (R_2 + x \sin \phi) h_{fg} \cos\phi \cos \alpha}{4 \mu_f (- a_1 \frac{z^3}{3} - b_1 \frac{z^2}{2})} \right]^{1/4} , \tag{23}$$

and was applicable from $z = 0$ to $z = z^* = z_0 - \delta^*/\cos \alpha$ (Figure 6).

Across the width of the trough, from $z = z_0$ to the mid-channel position,

$$h(x)_{trough} = \frac{k_f}{\delta^*(x)} . \tag{24}$$

26

$\delta^*(x)$ was considered constant across the trough width. Based

upon a check of the wall temperatures generated from Schafer's

computer program, the fluid temperature difference across the

width of the trough was predicted to be small. Fluid thermal

conductivity values were, therefore, assumed to remain

relatively constant. As a result, $h(x)_{trough}$ was assumed to

be constant across the trough width and was calculated using

equation (24) and a representative average inner wall temper-

ature to determine k_f.

An $h(z)$ temperature distribution was then needed

between $z = z^*$ and $z = z_o$. Since the thickness of condensate

film increased linearly from the value at z^* to the value at

z_o, the convective coefficient was assumed to decrease linearly

from $h(z^*)_{fin}$ to $h(x)_{trough}$.

Other boundary conditions were then applied in

accordance with the assumptions of Schafer, namely, zero heat

flux through the sides of the geometry, $T = T_s$ at the fin

apex, and constant convective coefficient, h_{out}, along the

outside surface of the wall. Boundary conditions for the

problem were, thus, completely specified.

In his expression for trough condensate cross-sectional

area, Schafer assumed that the surfaces of the condensate

flows from the fin and the trough were coincident at a position

directly above the trough-fin wall juncture (Figure 4). For

small fin film thicknesses and other than small fin angles,

this assumption was not accurate. In this study, it was

assumed that fin condensate thickness was much smaller than

27

trough condensate thickness. The trough condensate region
could, therefore, be more accurately described as shown in
Figure 6. The modified trough mass flow equation became

$$\dot{M}_{tot}(x) = \frac{\rho_f^2 \, \omega^2 \, (R_2 + x \, \sin \, \phi) \delta^*(x)^2 \, \sin \, \phi}{3\mu_f} \, (\delta^*(x)\epsilon + \delta^*(x)^2 \tan \alpha).$$

$$(25)$$

It should be noted that this equation differs from equation
(2) only in the expression for cross-sectional area of the
trough condensate region. The change in cross-sectional areas
involved the term, $1/\cos^2 \alpha$, which for large fin angles, could
make a significant difference in cross-sectional areas of the
two equations.

5. Condenser Heat Transfer Solution

Within the computer program, the heat transfer rate
for the entire condenser was determined by dividing its axial
length into one hundred equal length increments of length, Δx,
solving for the incremental heat transfer rate using an iter-
ative procedure, and summing those incremental rates to yield
a total heat transfer rate. A flowchart description of the
computer program used in this analysis is given in Figure 12.

At each increment, constants a_1 and b_1 were determined
using a Lagrangian interpolation fit of the temperatures
calculated from the previous iterate at nodes 1, 3, and 6.
For the first increment, a_1 and b_1 were initially calculated
from an initial guess of the temperatures at those nodes.
Convective coefficients at several locations along the fin
were determined using equation (23) and the linearly decreasing

28

h(z) assumption from z = z* to z = z_o. Next, average nodal

values, $h_{1\,avg}$, $h_{3\,avg}$, and the average h of the left hand

boundary region associated with node 6, (Figure 13), were then

calculated using the position dependent values of $h(z)_{fin}$ in

a Simpson's Rule approximation. $h(x)_{trough}$ was then calculated

from equation (24) using the δ* value calculated from the

previous increment. This value was used as the average

convective coefficient for nodes 9 and 12 and the right hand

boundary region of node 6. The average convective coefficients

calculated for the left and right hand boundary regions of

node 6 were then weighted by their respective region lengths.

The two values were then summed to yield the average convective

coefficient for node 6, $h_{6\,avg}$. The remaining boundary condi-

tions were then applied and incremental heat transfer rate

per unit condenser length, $\dot{Q}_j$, and nodal temperature values

were generated from the finite element subroutines.

If the resultant heat transfer rate converged to

within the criteria of 0.05 percent change from the value of

the previous iterate,

$$\left| \frac{\dot{Q}_j - \dot{Q}_{j-1}}{\dot{Q}_j} \right| < 0.0005 \, , \tag{26}$$

the incremental problem was deemed solved and $\dot{Q}_i$ set equal to

the final iterate, $\dot{Q}_j$. If, on the other hand, the convergence

criteria was not met, the newly calculated nodal temperature

values were used to establish a new set of inner wall

convective coefficients. After the remaining boundary

conditions had been applied, the finite element solution was
repeated until heat transfer rate converged to within the
acceptable 0.05 percent tolerance. Because $\dot{Q}_j$ was initial-
ized at zero for each increment, the iteration procedure was
repeated at least twice for every increment.

Incremental mass flow rate was then calculated using

$$\Delta \dot{M}_{tot_i} = 2 \frac{\dot{Q}_i}{h_{fg}} \Delta x . \qquad (27)$$

This value was then added to the mass flow rate from previous
increments. The subsequent interval's trough condensate
thickness was then calculated using a polynomial root-finder
subroutine to solve equation (25). The incrementation
continued until the entire length of the condenser had been
traversed. Incremental heat transfer rates were than summed
and a total heat transfer rate calculated from (3).

$$\dot{Q}_{tot} = 2 N_{fin} \sum_{i=1}^{100} (\dot{Q}_i \Delta x) , \qquad (28)$$

where N_{fin} was the number of fins along the inner wall
circumference.

To start the incrementation, two initial assumptions
were made. The initial increment's value of $\delta^* = \delta^*_1$ was
taken from the analysis of Schafer as 0.00006752 feet. For
reasons explained in the previous sub-chapter, a large variance
in the accuracy of this value would not significantly affect
the heat transfer results obtained from the computer program.

Additionally, at the first increment, initial guesses of fin temperatures at nodes 1, 3, and 6 were made in order to begin the solution. As an example, the temperatures used to begin the solution for the copper condenser with fluid saturation temperature of 200°F were T_1 = 200°F, T_3 = 195°F, and T_6 = 191°F.

For the copper condenser, the use of widely variant initial nodal temperature values, T_1 = 200°F, T_3 = 191°F, and T_6 = 182°F had little effect on convergence to the heat transfer solution for the first increment. However, as will be discussed in Chapter III, the initial temperature guess, coupled with the slight inaccuracy of the finite element nodal temperature solution produced numerical difficulties within the computer program for the stainless steel condenser.

III. DISCUSSION OF RESULTS

Computer results for the finned copper condenser were
generated for three outside convective coefficients, three
fin angles, and five rotation rates. The working fluid used
throughout the analysis was water. Representative results
are presented in Figures 14 and 16, 17, 18.

Figure 14 compares the heat transfer results of this
study with the results of the analysis of Schafer for given
operating conditions. It can be seen that the two-dimensional
conduction analysis allowing a parabolic temperature distri-
bution along the fin predicted heat transfer rates for the
finned condenser which are approximately seventy-five percent
greater than the rates predicted with the one-dimensional
model with linear temperature profile along the wall. This
rather significant change was unexpected, and may be some-
what in error due to numerical difficulties in the method.
These numerical difficulties arose due to the boundary
condition at node 1. The finite element boundary conditions
are established for each node such that the condition is
assumed to exist over the entire boundary region of the node.
Therefore, the zero flux boundary condition could not be
applied over the whole length of the left and right boundaries
of the condenser geometry. This problem existed for nodes 1,
4, 11, and 12, but was most critical for node 1 since it was
estimated that twenty to thirty percent of the total heat

flux through the inner wall passed through the region associated with this node.

An error of fifty percent in the calculation of node 1 heat transfer rate might then give a total heat transfer error of as high as fifteen percent. Two possible solutions to the boundary condition problem merit attention. The first is to increase the number of elements used in the solution of the geometry of Figure 6. However, a boundary region associated with node 1 would still exist on the left hand side of the geometry although reduced in size. The effects of the boundary condition problem would, therefore, be reduced but not eliminated.

The second solution would be to consider a wall geometry as shown in Figure 15. The zero flux boundary condition would then be forced along the boundary in question due to the symmetry of the problem. The use of one of these alternate solution methods might contain the added benefit of eliminating the numerical difficulties associated with the stainless steel condenser solution.

The heat transfer rate solution is generally affected in the same manner as with the analysis of Schafer when h_{out}, ω, and α were varied. In Figure 16 the influence of outside convective coefficient, h_{out}, is shown. Figure 17 illustrates how the rate of heat transfer was relatively unaffected as fin half angle, α, was varied. In addition, heat transfer rate was found not to vary significantly with rotation rate as shown in Figure 18. This result concurred with the results

33

obtained earlier by Schafer [8]. Schafer suggested that the invariance in heat transfer rate with the rotation rate was due to the cancelling effects of decreasing film thickness and decreasing temperature difference across the film thickness as rotation rate is increased.

Because of numerical difficulties in the program, no results were generated for the stainless steel condenser. With the solution of the first and second test cases, the nodal temperatures calculated were accurate only to within two or three degrees. In the condenser problem, this slight inaccuracy resulted in nodal temperatures along the fin wall which were slightly above the fluid saturation temperature. Computer output indicated that the wall temperature at node 3 was approximately 0.1°F above the saturation temperature when T_s = 200°F. As a result, the quantity within the brackets of equation (23) was a negative value. Error messages were generated when the computer attempted to evaluate the fourth root of this negative number.

IV. <u>CONCLUSIONS</u>

1. The addition of internal axial fins to the condenser surface of a rotating heat pipe significantly improves heat transfer performance.

2. Analysis of the condenser heat transfer problem using a two-dimensional wall conduction model and a parabolic temperature distribution along the fin yielded heat transfer rates about seventy-five percent above those predicted by the one-dimensional, linear temperature distribution analysis of Schafer [8].

3. For the geometrical cases studied in this thesis, the heat transfer rates calculated from the two-dimensional analysis are insensitive to changes in rotational speed and fin half-angle.

4. Boundary condition problems produced with the finite element solution for the copper condenser were the probable cause of solution inaccuracy on the order of fifteen percent.

5. Slight inaccuracy from the finite element calculation of nodal temperature values led to numerical difficulties in the heat transfer solution of the stainless steel condenser.

V.   RECOMMENDATIONS FOR FURTHER STUDY

It is suggested that the following topics be considered for future study of the internally finned, rotating heat pipe:

1.   Re-examination of the finite element analysis using either an increased number of elements for the geometry considered in this study or the mirror image geometry presented in Figure 15.

2.   Use of twelve-nodal elements in the finite element analysis to allow the assumption of a cubic inner wall temperature profile in order to more closely approximate the actual temperature distribution.

3.   Analysis of film condensation on a variety of fin shapes, and application of the solution to the two-dimensional model to determine the shape permitting optimum heat transfer rate.

4.   An experimental program in order to compare theoretical and experimental heat transfer rates of the internally finned condenser.
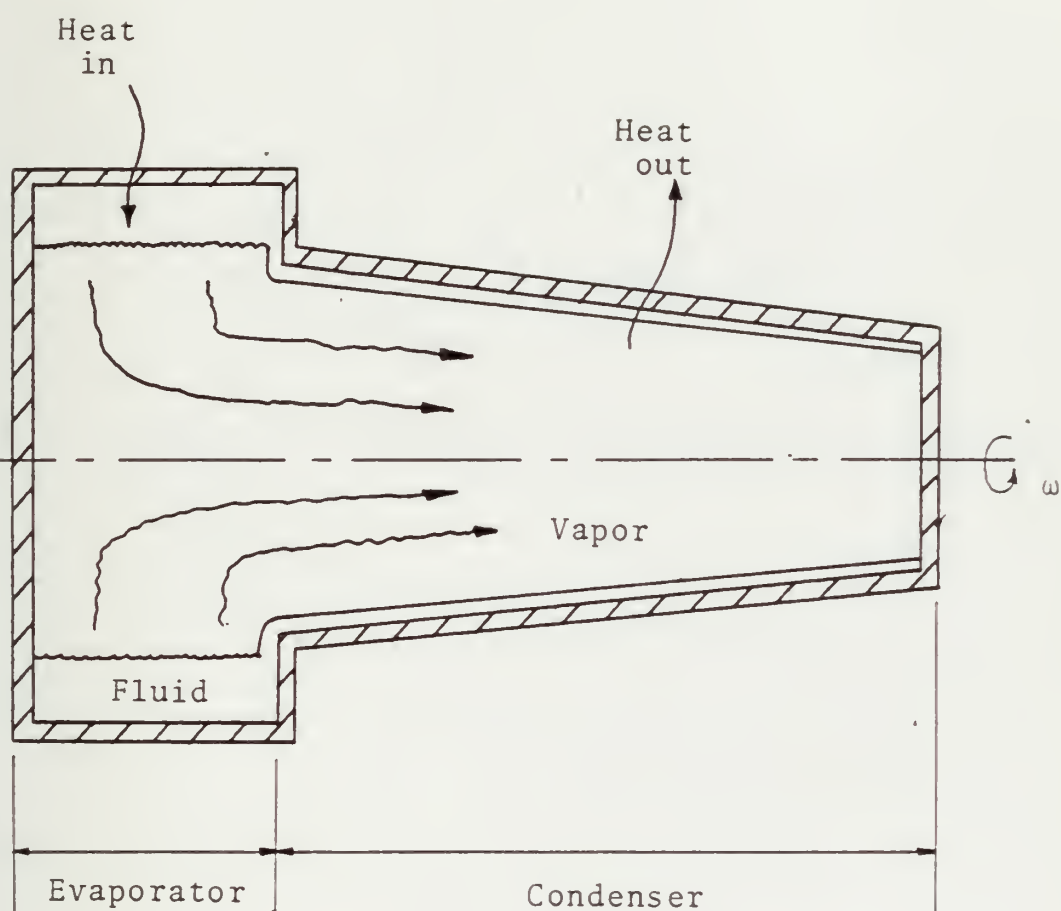
Figure 1. Rotating Heat Pipe Components
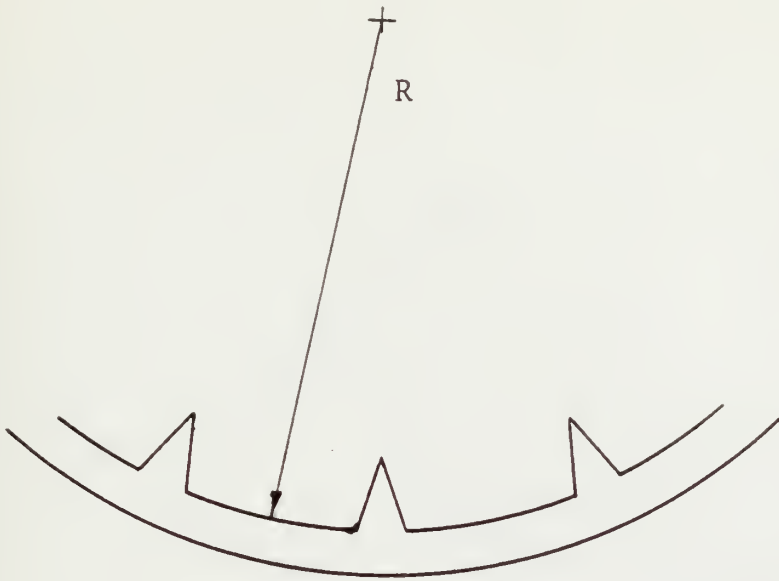
Figure 2a.   Internally Finned Condenser Geometry

$$r_1 = R_2 + x \sin \phi$$
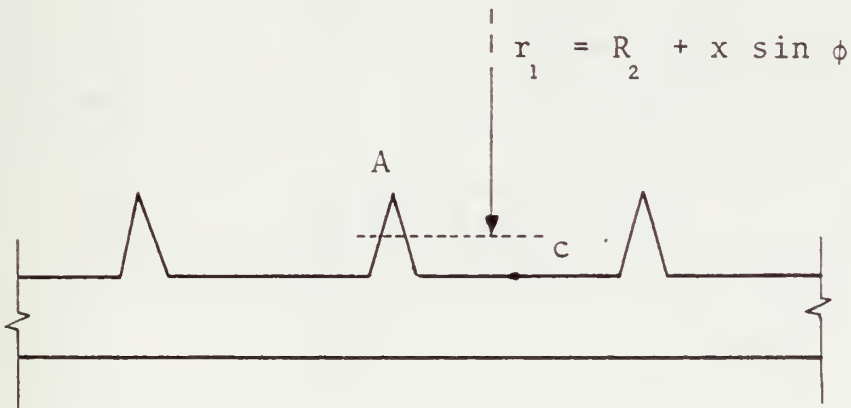
Figure 2b.   Planar Conduction Simplification
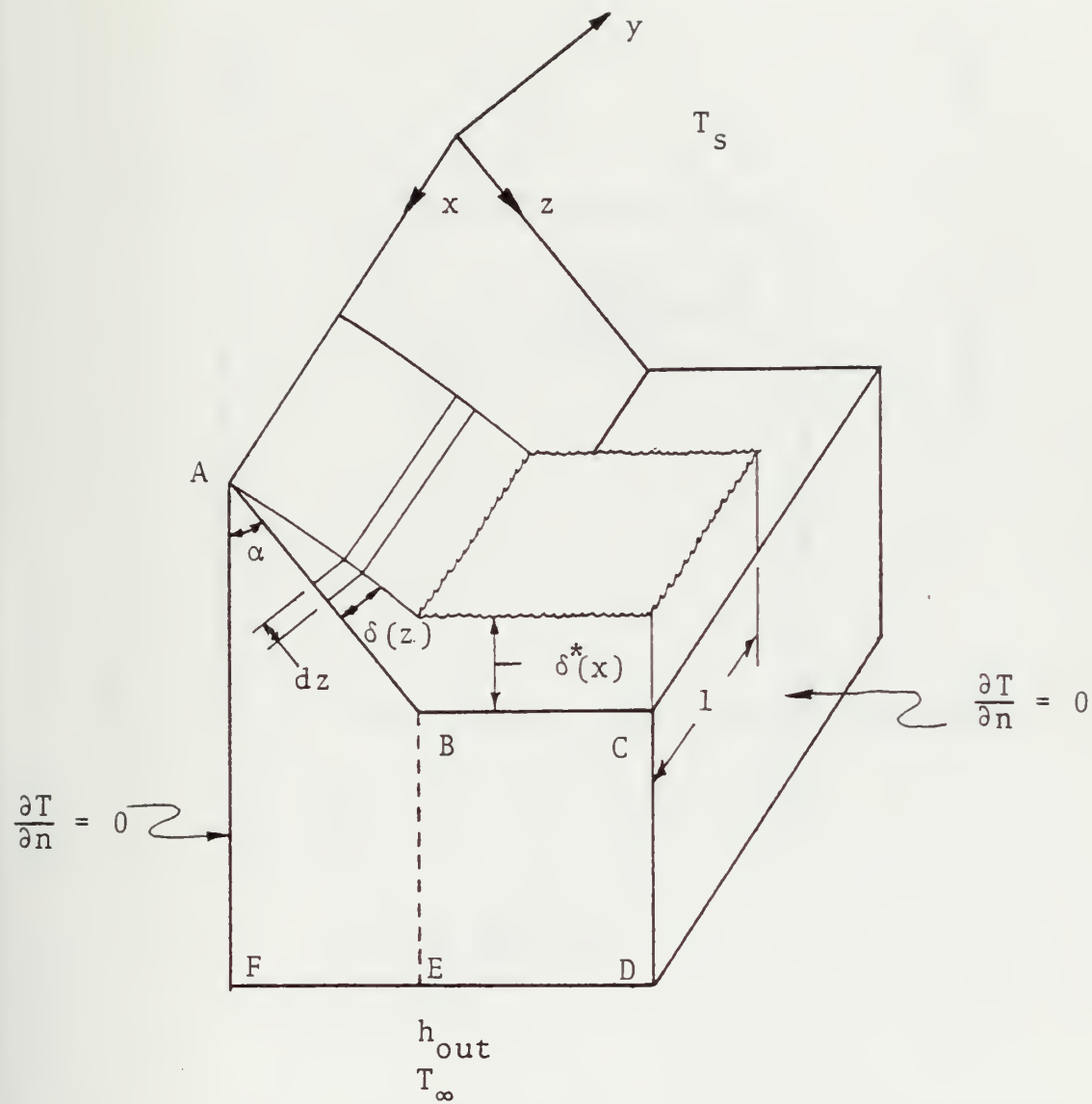
Figure 3.   Condenser Geometry Considered in Analysis
            of Schafer [8]

39

Figure 4. Condenser Geometry Considered in Analysis of Schafer [8]
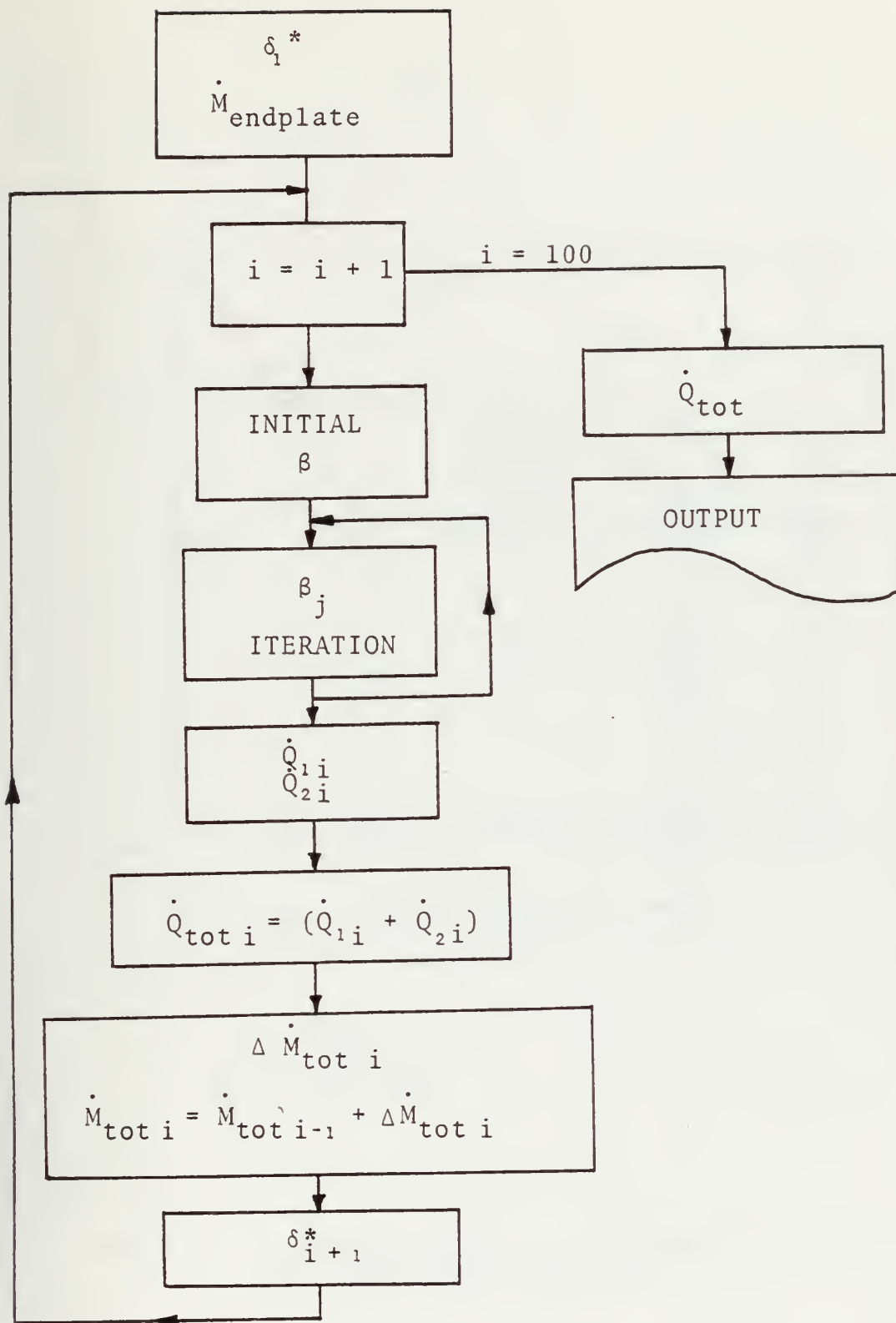
Figure 5. Computer Program Flowchart for the Analysis of Schafer [8]
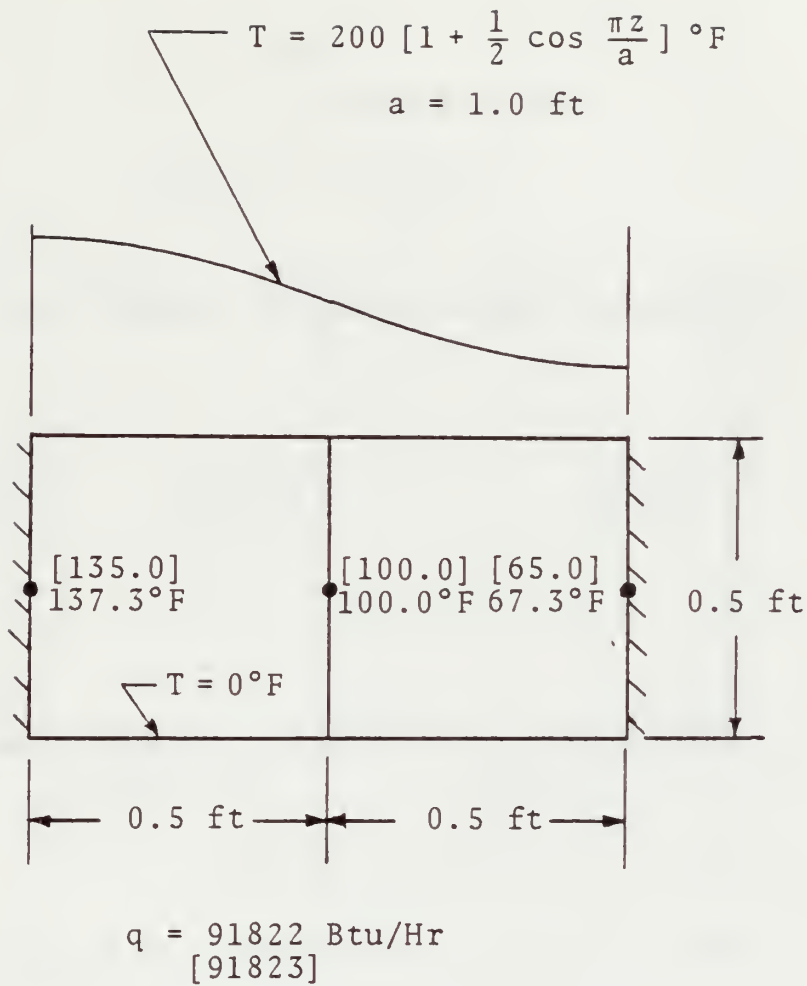
41

Figure 6. Condenser Geometry Considered in
Two-Dimensional Analysis

t = 0.03125 in.
b = 0.025 in.
R_2 = 0.762 in.
ϕ = 1°

$$T = 200 \left[1 + \frac{1}{2} \cos \frac{\pi z}{a} \right] \,^\circ F$$

$$a = 1.0 \text{ ft}$$

[135.0]
137.3°F

[100.0] [65.0]
100.0°F 67.3°F

0.5 ft

T = 0°F

0.5 ft

0.5 ft

q = 91822 Btu/Hr
[91823]
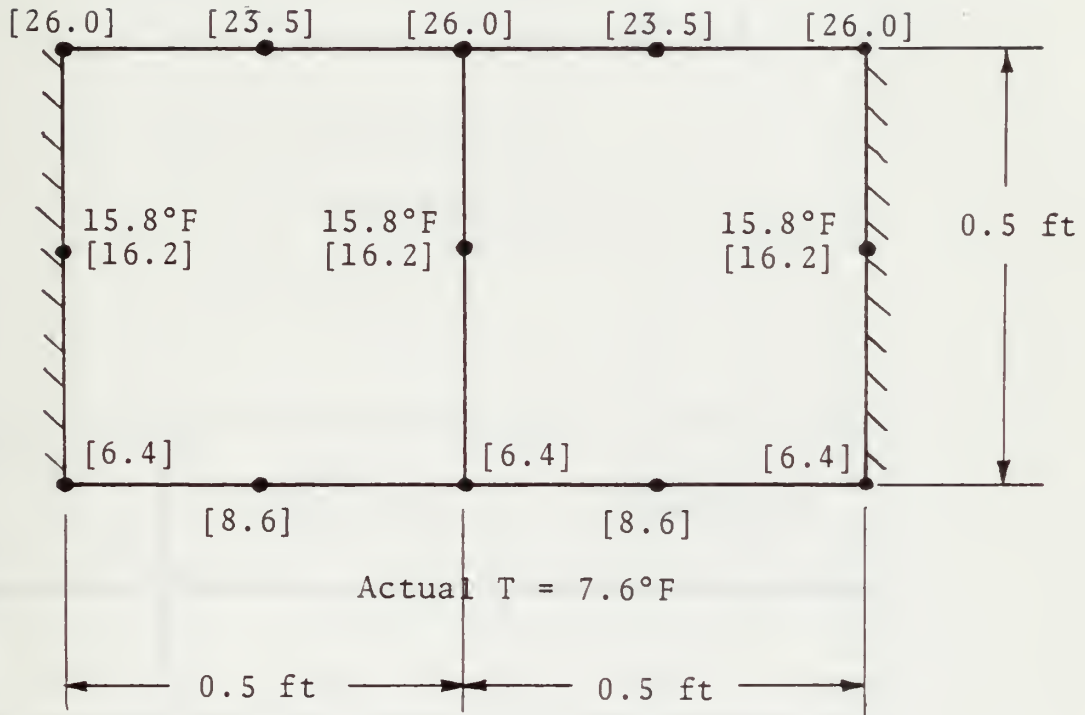
Figure 7. Test Case (1)

Figure 8. Test Case (2)

$$T_{\infty 1} = 200°F$$
$$h_1 = 100 \text{ Btu/Hr-ft}^2\text{-}°F$$

1.0 ft

0.5 ft

$$\leftarrow c \rightarrow \quad \frac{0.75\text{-}c}{\text{ft}}$$
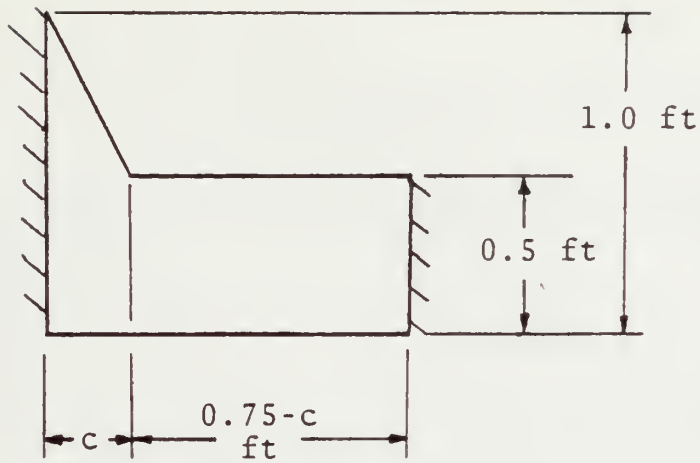
$$h_2 = 1000 \text{ Btu/Hr-ft}^2\text{-}°F$$

$$T_{\infty 2} = 100°F$$

q\\c	One-Dimensional	Two-Dimensional
0.25 ft	6526	6727
0.05 ft	6561	6754

Figure 9. Test Case (3)

$T_{\infty 1} = 200°F$

$h_1 = 100 \ Btu/Hr-ft^2-°F$

1.0 ft

0.5 ft

0.25 ft

0.5 ft
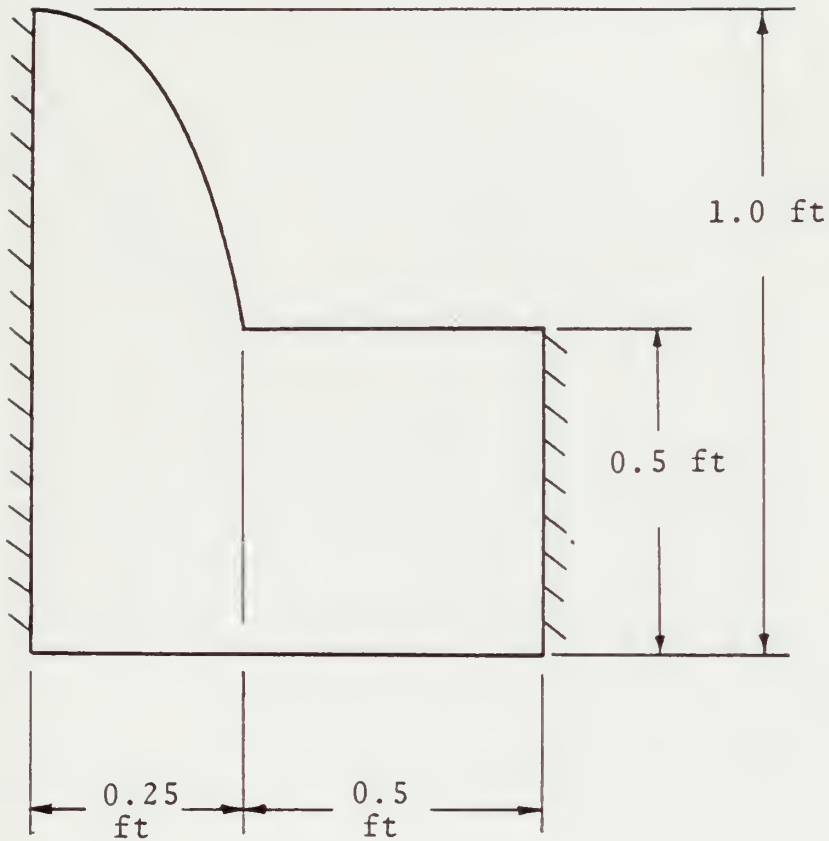
$h_2 = 1000 \ Btu/Hr-ft^2-°F$

$T_{\infty 2} = 100°F$

$q = 6563 \ Btu$
[6921]

Figure 10.   Test Case (4)

$T_{\infty 1} = 200°F$
$h_1 = 100$ Btu/Hr-ft^2-°F

1.0 ft

0.5 ft

0.25
ft

0.5
ft
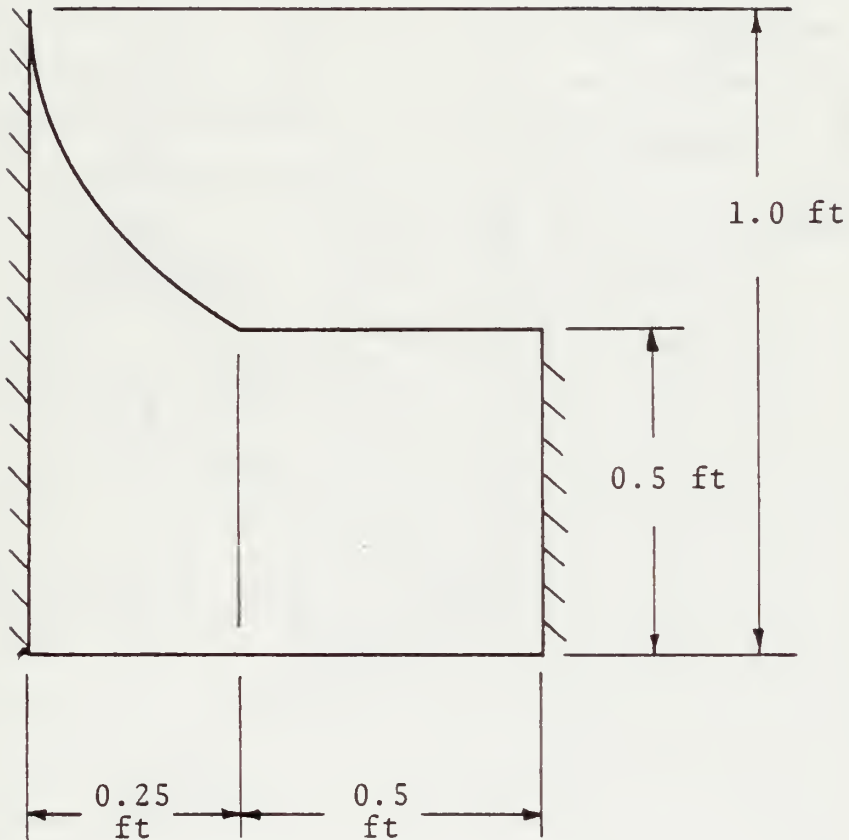
$h_2 = 1000$ Btu/Hr-ft^2-°F

$T_{\infty 2} = 100°F$

$q = 6336$ Btu/Hr
[6548]

Figure 11. Test Case (5)

$$\delta^*_1, \ T_{node_1}$$

$$i = i + 1$$

$$i = 100$$

$$h(z)_{fin}$$
$$h_{trough}$$

FINITE
ELEMENTS
SUBROUTINES
$$\dot{Q}_j, \ T_{node\ j}$$

$$\left| \frac{\dot{Q}_j - \dot{Q}_{j-1}}{\dot{Q}_j} \right| < 0.0005$$

No

Yes

$$\Delta\dot{M}_{tot\ i}$$
$$M_{tot\ i}$$
$$\delta^*_{i+1}$$

$$\sum_{i=1}^{100} Q_i \ \Delta x$$

OUTPUT
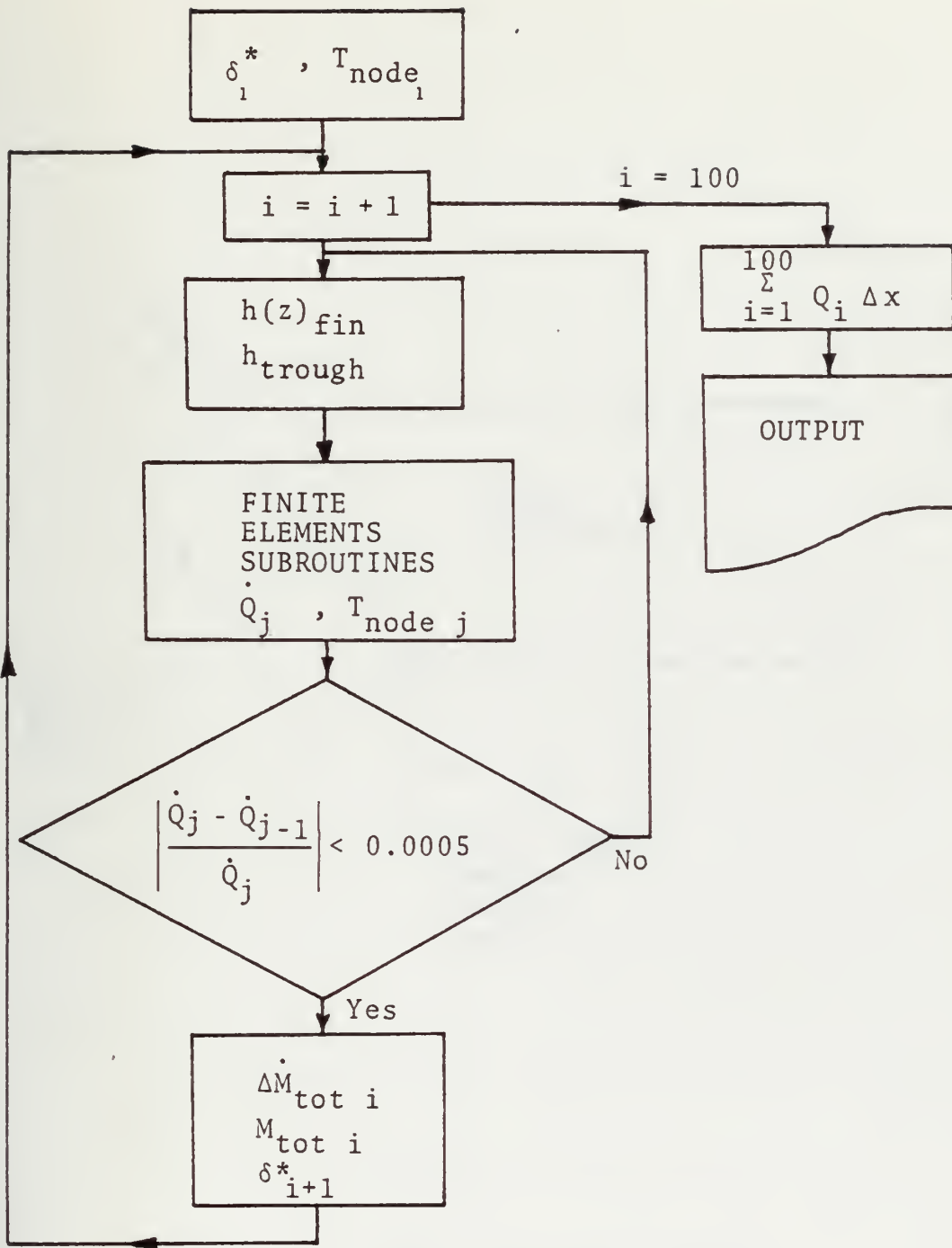
Figure 12.   Computer Program Flowchart of
Two-Dimensional Conduction Analysis
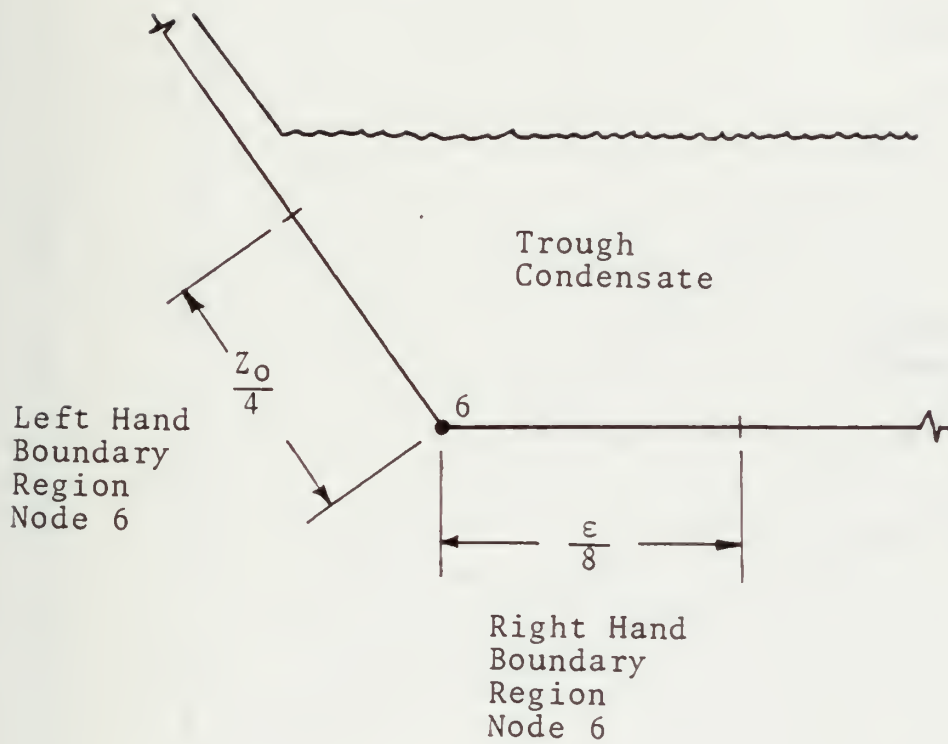
Figure 13. Node 6 Boundary Regions
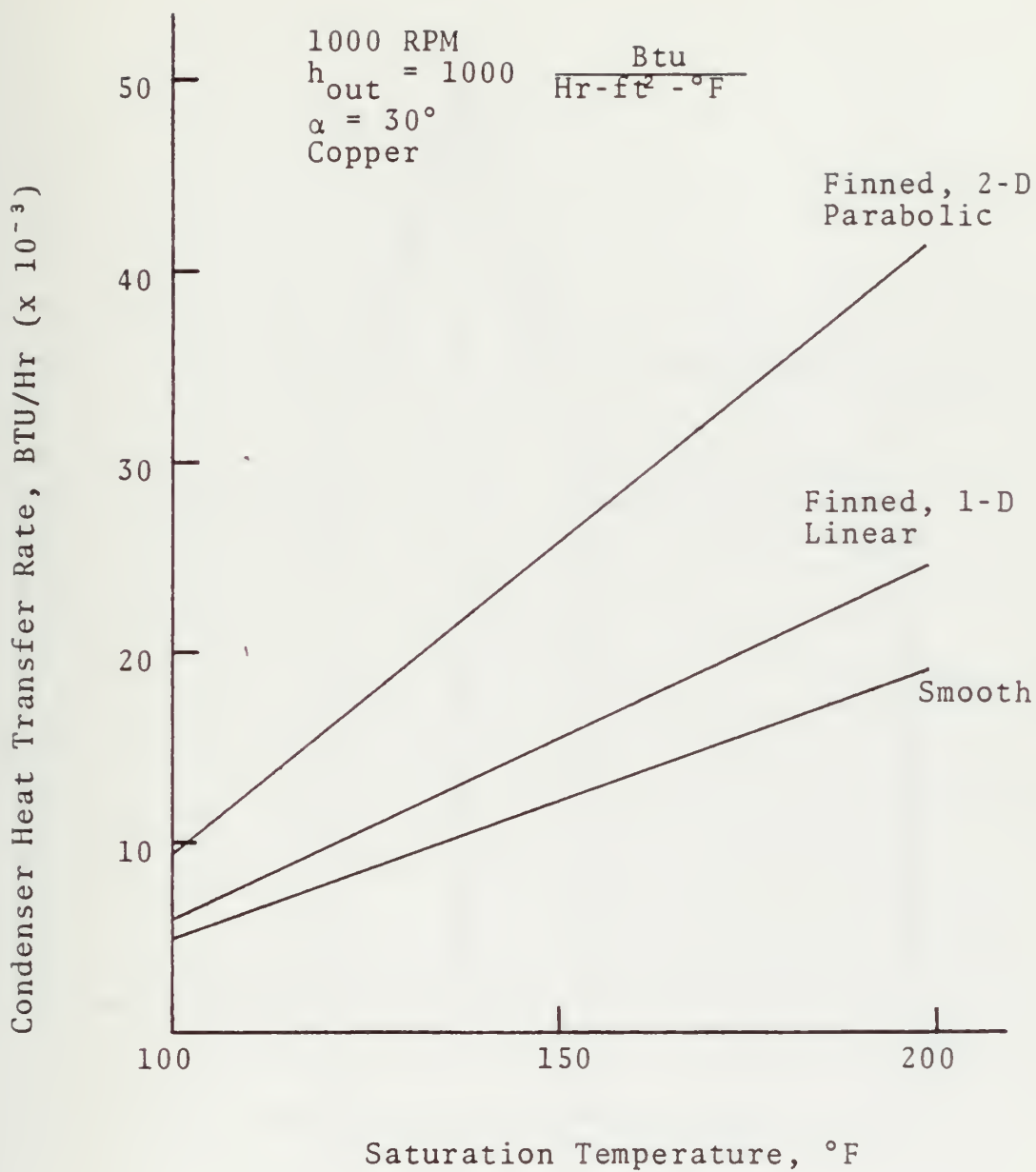
Figure 14.   Condenser Heat Transfer Rate vs.
             Saturation Temperature
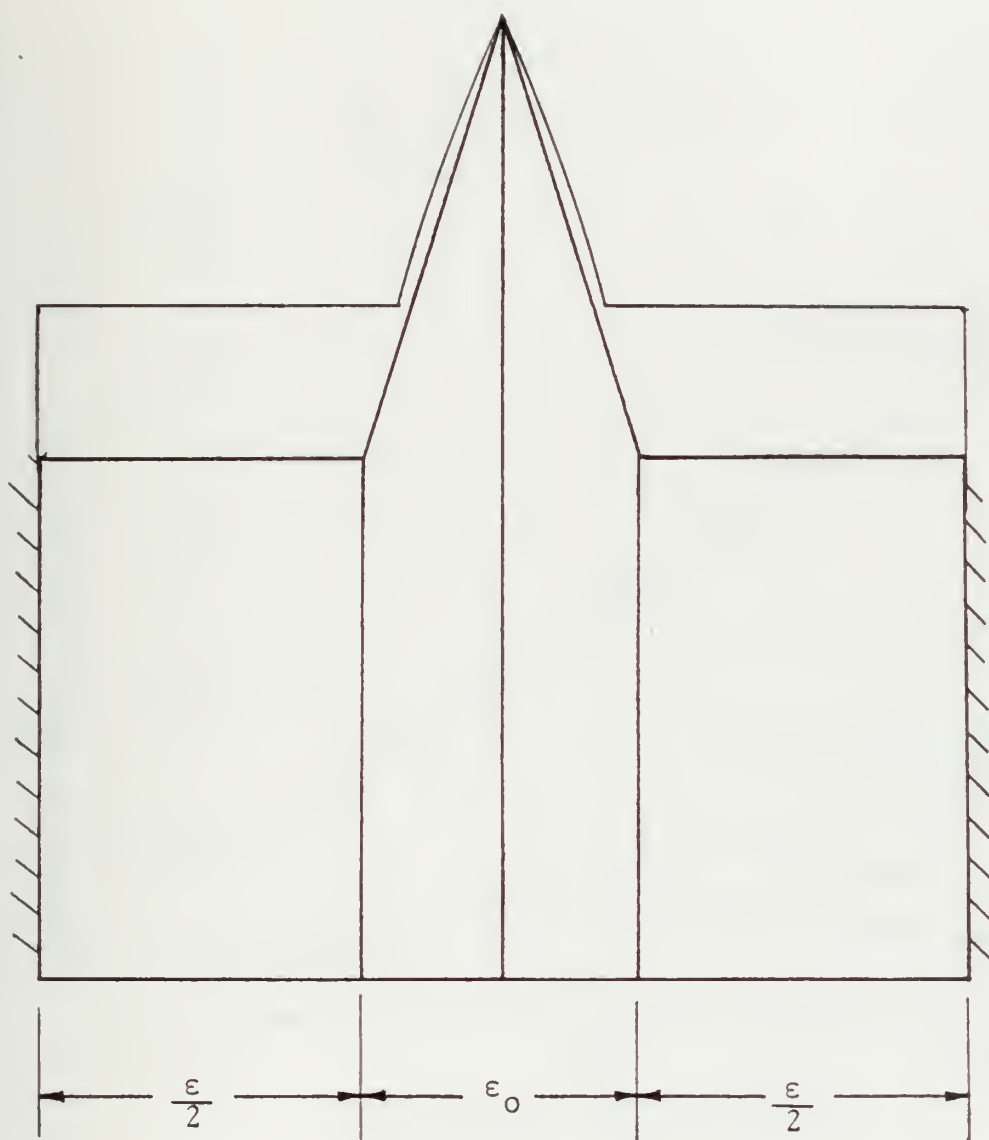
Figure 15.   Alternate Condenser Wall Geometry
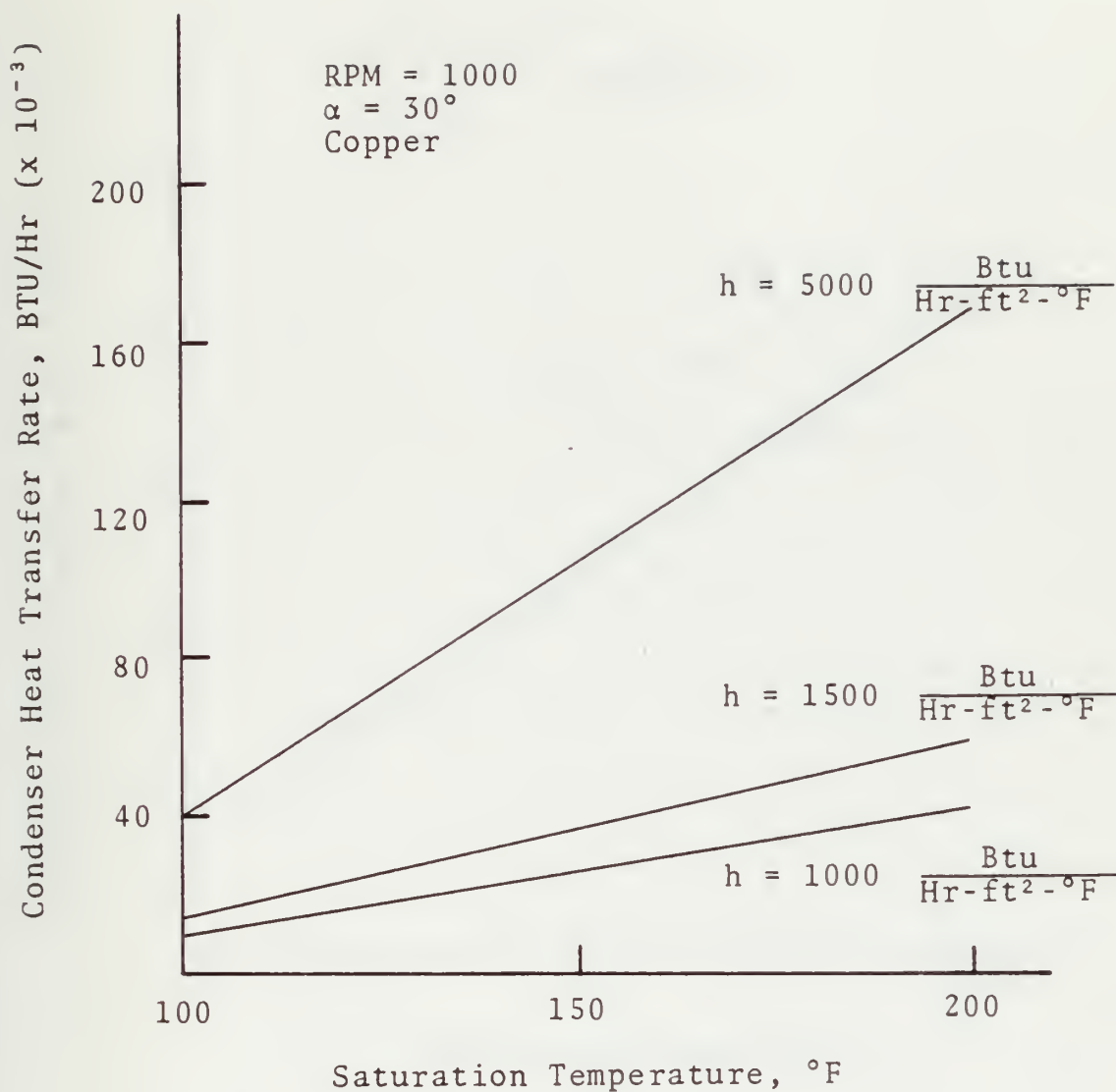
Figure 16.   Condenser Heat Transfer Rate vs.
Saturation Temperature
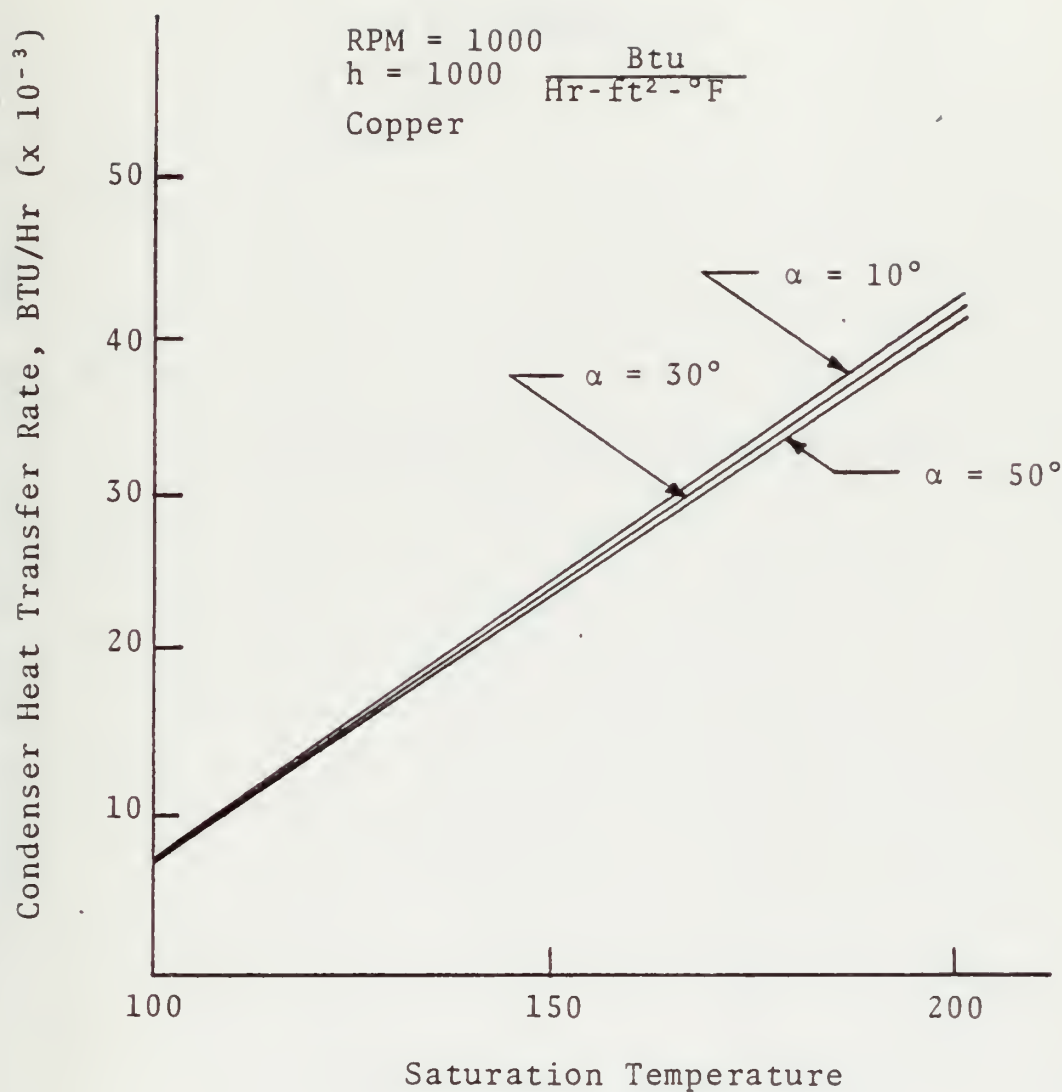
Figure 17.   Condenser Heat Transfer Rate vs.
            Saturation Temperature
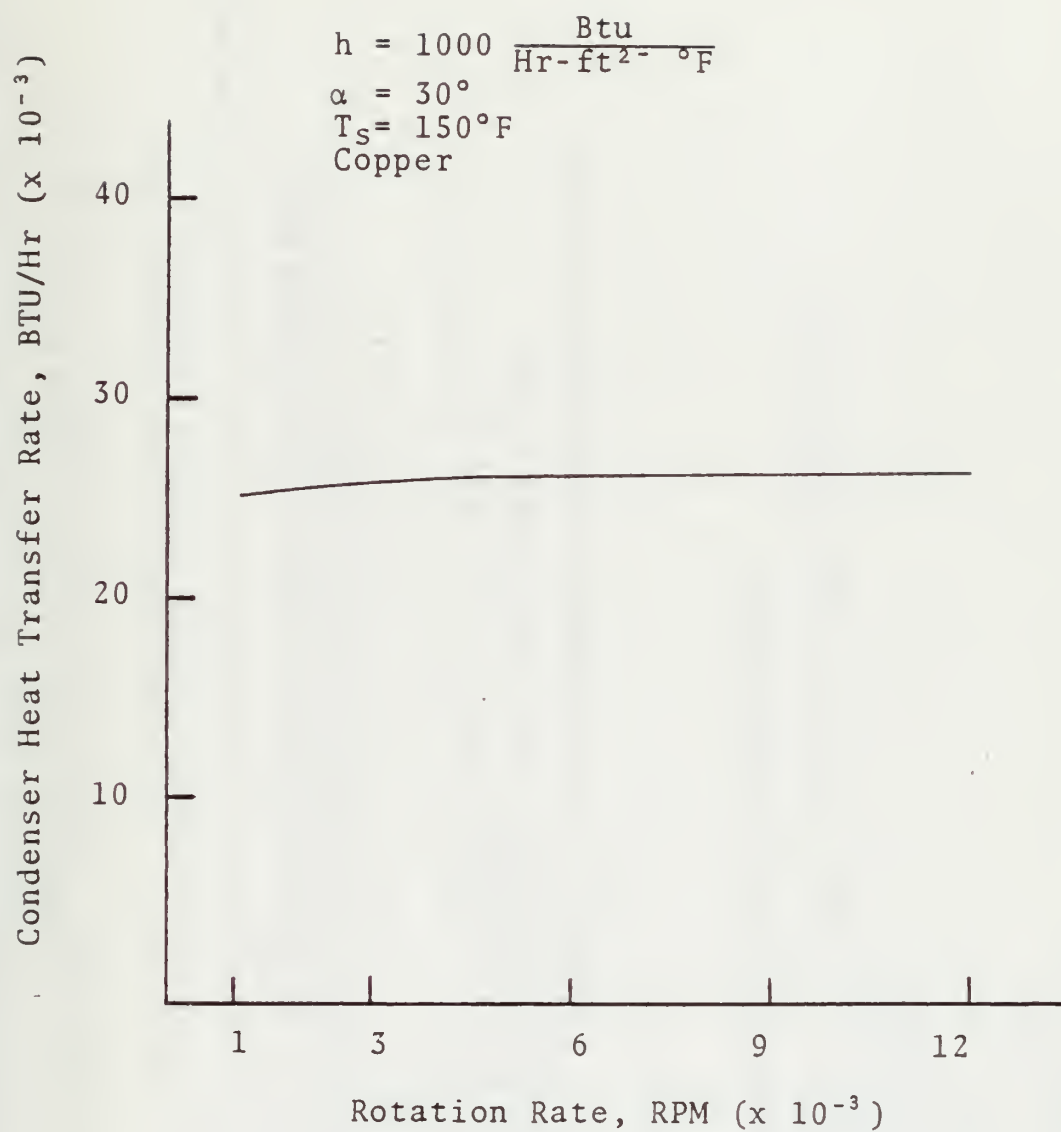
Figure 18.   Condenser Heat Transfer Rate vs.
Rotation Rate

```
C************************************************************************
C*    THE DIMENSIONAL HEAT CONDUCTION FINITE ELEMENTS ANALYSIS
C*    CF A ROTATING HEAT PIPE.  COMPILED BY ENSIGN ROBERT C. CORLEY IN
C*    JUNE, 1976
C*
C*    BASED UPON AN ADAPTATION OF THE THREE-DIMENSIONAL ISOPARAMETRIC
C*    FINITE ELEMENTS PROGRAM COMPILED BY LCDR GIRARD T. LEW IN
C*    DECEMBER, 1972.
C************************************************************************
      IMPLICIT REAL*8(A-H,O-Z)
      DIMENSION EPS(101),R(101),DELST(102),T8(101),RHOF(101),CF(101),
     1VISF(101),TOT(101),TMASS(101),XCOF(5),COF(5),ROOTR(4),
     2FE(4),TNODE(13),CORD(8,2),ENN(6,8),DCCL(8,2),AJ(2,2),AJI(2,2),
     3WRK(13),FE(8),BGM(13,8),COARD(13),F(13),FHI(13),
     4FHIWRK(101),HAVG(101),T6(101),T7(101),T12(101),
     5T4(101),T11(101),PWRK(101)
      COMMON /MTRX/ CORC(8,2),ENN(8,8),CCCL(8,2),AJ(2,2),AJI(2,2),
     1FE(8,8),FE(8),BGM(13,8),COARD(13),F(13),FHI(13),
     2FHIWRK(13),HAVG(13),TCT(101)
      COMMON /FLP/DTJ,AK,TINF,APZRC,ABIGN,TSAT,HCAVG,CCNVER
      COMMON /IMTRX/ NCON(28)
      DIMENSION NCON(2,8)
      FLEN(A1,B1,ZZ)=(-1.0D0*(A1*ZZ**3/3.0D0+B1*ZZ**2/2.0D0))**0.25D0
      DO 60 J=1,2
      DO 60 I=1,8
   60 READ (5,65) NCON(J,I)
   65 FORMAT (I5)
   80 CONTINUE
C
C     INITIAL TEMPERATURE ESTIMATE (INNER NODES)
C
      DO 416 KJI=1,3
      READ (5,15) TNODE(1),TNODE(3),TNODE(5),TNODE(6),TNODE(5),TNODE(12)
   15 FORMAT (5F10.0)
      PHI1=1415.265385875D0
      APHI=2.0D0*PI/360.0D0
      SPHI=DSIN(APHI)
      TPHI=DCTAN(APHI)
      CELX=0.75D0/100.0D0
      RE2=0.162C0/12.0D0
      THICK=0.0031250/12.0D0
      CEASE=2.0D0*PI*0.75C0/12.0D0
      REXIT=0.775D0+9.0C0*TPHI
```

```
      CEXIT=2.0C0*PI*REXIT/12.0D0
CC    416,KJK=1,9
      REAL(5,10) ANGLE,TSAT,HOUT
   10 FCRMAT(3F10.0)
      HFG=1097.2C0-0.601875D0*TSAT
      ALFA=ANGLE*APHI
      CALFA=CCOS(ALFA)
      SALFA=CSIN(ALFA)
      TALFA=CTAN(ALFA)
      EZERO=0.25C0/12.0C0
      NFIN=CBASE/(2.0D0*BFIN*TALFA)
      EPSEX=(CEXIT-2.0D0*EZERO)/NFIN
      BETA=416*ARPM*2.0D0*EZERO)/100C.3000
      OMEGA=NRPN*2.0D0*PI*60.0D0
      CELST(1)=0.0000675200
      CICT=0.0C0

C     CCRDINATE MATRIX VALUES (CCARD(Z,Y))
C
      CCARD(1,1)=0.0D0
      CCARD(1,2)=BFIN+THICK
      CCARD(2,1)=0.0D0
      CCARD(2,2)=COARD(1,2)/2.0D0
      CCARD(3,1)=0.0D0
      CCARD(3,2)=THICK+BFIN/2.0D0
      CCARD(4,1)=0.0D0
      CCARD(4,2)=EZERO/4.0D0
      CCARD(5,1)=0.0D0
      CCARD(5,2)=EZERO/2.0C0
      CCARD(6,1)=0.0D0
      CCARD(6,2)=THICK
      CCARD(7,1)=0.0D0
      CCARD(7,2)=EZERO/2.0D0
      CCARD(8,1)=COARD(7,1)
      CCARD(8,2)=COARD(6,2)/2.0D0
      CCARD(9,1)=THICK
      CCARD(11,2)=0.0D0
      CCARD(11,2)=THICK
      CCARD(12,2)=THICK/2.0D0

      ZZERO=BFIN/CALFA
      ZL=EZERC/2.0D0
      HAVG(2)=0.0D0
      HAVG(4)=HOUT*ZL/4.0C0
```

```
      HAVG(5)=HGLT*ZL/2.0D0
      HAVG(8)=0.0D0
C
C     LENGTH INCREMENTS
C
      DO 5500 III=1,101
      TCT(III)=1.0D0
      EPS(III)=EZERO+BETA*III
      ZCHAN=EPS(III)/2.0D0
      COARC(9,1)=(EZERO+ZCHAN)/2.0D0
      COARC(10,1)=COARD(9,1)+ZCHAN/2.0D0
      COARC(12,1)=COARD(11,1)
      COARC(11,1)=COARD(11,1)/4.0D0
      HAVG(7)=HOUT*(ZCHAN+ZL)/4.0D0
      HAVG(10)=HOUT*ZCHAN/2.0D0
      TSCLID=(TINF+TSAT)/2.0D0
      R(III)=R2+III*DELX*SPHI
      GO TO 20
C
C     FINITE ELEMENTS:  ITERATE UNTIL CONVERGENCE CRITERIA IS MET
C
   5  JJJ=JJJ+1
      IF(JJJ.LE.10) GO TO 36
      WRITE(6,57)
  57  FORMAT(4X,'DIVERGING OR SLCWLY CONVERGING SOLUTICN')
      GO TO 5500
  36  DO 30 IT=1,13
      TNODE(IT)=PHI(IT)
  30  CONTINUE
      TSCLID=(TNODE(2)+TNODE(8)+TNODE(13))/3.0D0
  20  DO 25 IT=1,13
      PHI(IT)=0.8D0
  25  CONTINUE
C
C     SOLID-FLUID PROPERTIES
C
      TFILM=(TNODE(1)+TNODE(3)+TNODE(6)+TNODE(9)+TNODE(12)+5.0D0*TSAT)/1
     10.0D0
      CF(III)=0.3034D0+0.0007389270D0*TFILM-0.0000014732100*TFILM**2
      CW(III)=231.7772D0-0.02222D0*TSCLID
      AK(III)=...
      RTOF(III)=62.774D0-0.0025569800*TFILM-0.0000525720D0*TFILM**2
      VISF(III)=0.001397D0-C.0001466D0*TFILM+0.0000000653125300*TFILM**3
     12=0.0000000009765600*TFILM**3
      VISF(III)=VISF(III)*3600.0D0
```

```
C
C     PARABOLIC TEMPERATURE DISTRIBUTION ALONG THE FIN WALL
C
      CNST=(CF(III)**3*RHOF(III)/VISF(III))**2*OMEGA**2*(R(III))*HFG*CALFA*CPHI/
     1(4.0D0*VISF(III))**0.25D0
      ZA=ZZZERO*0.25D0
      ZE=ZZZERO*0.75D0
      ZC=ZZZERO*0.875D0
      ZB=ZZZERO/2.0D0
      ZSTAR=ZZERO-DELST(III)/CALFA
      IF(ZSTAR.GT.ZB) GO TO 172
      ZCNE=(ZSTAR+ZA)/2.0D0
      CELZ1=(ZSTAR+ZA)
      CELZ2=ZE-ZA
      GO TO 174
  172 ZCNE=(ZE+ZSTAR)/2.0D0
      CELZ1=ZCNE-ZB
      CELZ2=ZE-ZSTAR
      A1=2.0D0*(TNODE(1)-2.0C0*TNODE(3)+TNODE(6))/ZZERO**2
      B1=2.0D0*(-1.5D0*TNODE(1)+2.0D0*TNODE(3)-0.5C0*TNODE(6))/ZZERO
  174 HNODA=CNST/HDEN(A1,B1,ZA)
      HNODCC=CNST/HDEN(A1,B1,ZC)
      HNODZ1=CNST/HDEN(A1,B1,ZONE)
      HNODZS=CNST/HDEN(A1,B1,ZSTAR)
      HCAVG=CF(III)/DELST(III)
      AA1=(HCAVG-HNODZS)/(Z6-ZSTAR)
C
C     AVERAGE NODAL CONVECTIVE COEFFICIENT DETERMINED ALONG THE
C     FIN WALL
C
      IF(ZSTAR.GT.ZB) GO TO 176
      HAVG(3)=(DELZ1/3.0D0)*(HNODA+4.0C0*HNODZ1+HNODZS)+((AA1*CELZ2+2.0C
     10+HNODZS)/2.0D0)*CELZ2
      HAVG(6)=(ZZERO/4.0D0)*(AA1*CELZ2+HNODZS+HCAVG)/2.0D0
      GO TO 178
  176 HAVG(3)=(ZZERO/12.0D0)*(HNODA+4.0C0*HNODZ3+HNODE)
      HAVG(6)=(DELZ1/3.0C0)*(HNODB+4.0C0*HNODZ1+HNODZS)+(HNODZS+HCAVG)*C
  178 HCAVG=HCAVG*ZCHAN/4.0D0
      HAVG(2)/2.0D0
      HAVG(9)=2.0D0*HCAVG
      HAVG(12)=HCAVG
C
C     FORM THE COMPONENTS OF THE VECTOR "F"
C
      F(1)=0.0D0
```

```
      F(2)=0.0D0
      F(3)=-HAVG(3)*TSAT
      F(4)=-HAVG(4)*TINF
      F(5)=-HAVG(5)*TINF
      F(6)=-1.0D0*(HAVG(6)+HCAVG)*TSAT
      F(7)=-HAVG(7)*TINF
      F(8)=0.0D0
      F(9)=-HAVG(9)*TSAT
      F(10)=-TAVG(10)*TINF
      F(11)=-TAVG(11)*TINF
      F(12)=-TAVG(12)*TSAT
      F(13)=0.0D0
C
C     INITIALIZE "PHI" AND "PHIWRK"
C
      DO 633 IJ=1,13
      PHI(IJ)=0.0D0
      PHIWRK(IJ)=0.0D0
  633 CONTINUE
C
C     *******************************************************************
C     ******************* ENTRY INTO THE FINITE ELEMENTS SECTION
C     *******************************************************************
      CALL MERGE
      CALL STEADY(III)
C
C     *******************************************************************
C     ******************* EXIT FROM THE FINITE ELEMENTS SECTION **********
C     *******************************************************************
      IF (CONVER.GT..0.000500) GO TO 5
      T4(IIII)=PHI(4)
      T6(IIIII)=PHI(6)
      T7(IIIIII)=PHI(7)
      T11(IIIIIII)=PHI(11)
      T12(IIIIIIII)=PHI(12)
      PHWRK(IIII)=PHIWRK(1)*DELX
      TCT(IIII)=TOT(III)*DELX
      STO=QTCT(III)+TCT(III)
      FLCQ=QTCT(III)*2.0D0/HFG
      IF(III.GT.1) GO TO 9200
      C1==(RHOF(III)*OMEGA)**2
      C2=R2*SFHI/(3.0D0*VISF(III))
      C33=EZEFC*DELST(1)**3+TALFA*CELST(1)**4
      FLCW1=C1*D2*D3
      TMASS(1)=FLOW1+FLOW
      GO TO 9300
 9200 TMASS(III)=TMASS(III-1)+FLOW
C
```

```
C    FINC THE NEXT ITERATE CF TROUGH CONCENSATE THICKNESS
C
5200  N=4
      XCCCF(1)=-TMASS(III)
      XCCCF(2)=0.0C0
      XCCCF(3)=0.0C0
      C1=(RHOF(III)*OMEGA)**2*R(III)*SFI/(3.0C0*VISF(III))
      XCCCF(4)=C1*EPS(III)
      XCCCF(5)=C1*TALFA
      IER=0
      CALL   DPCLRT(XCCF,CCF,M,ROOTR,ROOTI,IER)
      IF (ROOTR(1).LT.-0.005D0.AND.ROOTR(1).GT.0.0C0) GO TO 9310
      IF (ROOTR(2).LT.-0.005D0.AND.ROOTR(2).GT.0.0C0) GO TO 9320
      IF (ROOTR(3).LT.-0.005D0.AND.ROOTR(3).GT.0.0C0) GO TO 9330
      IF (ROOTR(4).LT.-0.005D0.AND.ROOTR(4).GT.0.0C0) GO TO 9340
      GO TO 9500
9310  DELST(III+1)=ROOTR(1)
      GO TO 9500
9320  DELST(III+1)=ROOTR(2)
      GO TO 9500
9330  DELST(III+1)=ROOTR(3)
      GO TO 9500
9340  DELST(III+1)=ROOTR(4)
9500  CCNTINUE
      CTCT=QTCT*NFIN*2.0C0
C
C     CUTFUT
C
C
9225  WRITE (6,9225) HFG,CTCT,NFIN,ANGLE,HOUT,TSAT,NRPN
      FORMAT(1H ,//,4X,'HFG=',F7.2,/,4X,'Q TOTAL=',F5.1,/,4X,'NUMBER C
     1FFINS=',I6,/,4X,'HALF ANGLE OF GROOVE=',F5.1,/,4X,'HEAT TRANSFER
     2COEFFICIENT=',F7.1,/,4X,'SATURATION TEMP=',F6.1,/,4X,'RPN=',I6)
9250  WRITE(6,9250) J,'0',6X,J,'',4X,'FILM THICKNESS',6X,'Q-INCREM',6X,'MASS-TOT',
     18X,'T4',5X,T6,5X,T7,5X,'T11')
      WRITE(6,9255)(III,DELST(III),TOT(III),TMASS(III),T4(III),T6(III),
     1T7(III),T11(III))
9255  FORMAT(1H ,4X,I4,4X,F12.10,4X,F10.4,6X,F5.5,6X,F5.1,6X,F5.1,6X,F5
     1.1,6X,F5.1)
9600  CCNTINUE
9260  WRITE(6,9260) J,6X,J,6X,'K-WALL',4X,'K-FILM',3X,'CENSITY',4X,'VISC-FI
     1LM',6X,'EPSILON',5X,'RADIUS',7X,'T12',3X,'G-BCT')
      WRITE(6,9100) III,CM(III),CF(III),RHOF(III),VISF(III),EFS(III),R(
     1III),T12(III),PWRK(III))
9100  FORMAT(1H ,4X,I4,4X,F7.3,4X,F6.4,4X,F6.3,4X,F5.7,4X,F9.7,4X,F7.5,
```

```
      15X,F5.1,1X,1P1D12.3)
9600  CONTINUE
9416  CONTINUE
9500  WRITE(6,9910)CRASH,CRASH,CRASH
9510  FORMAT(3X,'CRASH,CRASH,CRASH')
      STOP
      END
      SUBROUTINE MERGE
      IMPLICIT REAL*8(A-H,O-Z)
      COMMON /MTRX/ CORC(8,2),ENN(8,8),CCOL(8,2),AJ(2,2),AJI(2,2),
     1ENW(8,8),FE(8),BGM(13,8),COARD(13,2),TOT(101),F(13),FHI(13),
     2PHIWRK(13),HAVG(13),TOT(101)
      COMMON /FLP/ DTJ,AK,TINF,APZRO,AEIGN,TSAT,HCAVG,CCNVER
      COMMON /IMTRX/ NCON(2,8)
C
C     ZERO THE MASTER MATRIX
C
      DO 1000 I=1,13
      DO 1000 J=1,8
1000  BGM(I,J)=0.0D0
C
C     ZERO THE ELEMENT WORKING MATRICES
C
      DO 8000 I=1,2
      DO 1100 II=1,8
      DO 1110 JJ=1,2
1110  CORC(II,JJ)=0.0D0
      DO 1100 JI=1,8
1100  ENW(II,JI)=0.0D0
      DO 1200 K=1,2
      INCX=NCON(I,J)
1200  CORC(J,K)=COARD(INCX,K)
C
C     FORMING THE ELEMENTAL "H" MATRIX
C
C     CALL SCLARE
C
C     ASSEMBLE THE "H" MATRIX
C
6000  DO 7000 II=1,8
      ICZ =NCON(I,II)
      DO 7000 JJ=1,8
      ICY=NCON(I,JJ)-IDZ+1
      IF(ICY.LT.1) GO TO 7000
      BGM(IDZ,IDY)=BGM(ICZ,IDY)+ENW(II,JJ)
7000  CONTINUE
8000  CONTINUE
```

```
      DO 9000 IH=2,12
 9000 BGM(IH,1)=BGM(IH,1)+HAVG(IH)
      CONTINUE
      BGM(6,1)=BGM(6,1)+HCAVG
      RETURN
      END
      SUBROUTINE STEADY(III)
      IMPLICIT REAL*8(A-H,O-Z)
      COMMON /MTRX/ CORD(8,2),ENN(8,8),CCOL(8,2),AJ(2,2),AJI(2,2),
     1ENW(8,8),FE(8),BGM(13,8),COAR(13,2),F(13),PHI(13),
     2PHIWRK(13),HAVG(13),TOT(101)
      COMMON /FLP/ DTJAK,TINF,APZRO,AEIGN,TSAT,HCAVG,CCNVER
      COMMON /IMTRX/ NCON(2,8)
C     SOLVING THE STEADY STATE PROBLEM OF THE FORM (H)*<PHI>+<F>=0
C     USING SUBROUTINES "LDLT" & "SLV"
C
C     APPLY THE SPECIFIED NODAL VALUE, PLACE "F" ON RIGHT HAND SIDE
C     STORE "F" FOR REFERENCE
      PHI(1)=TSAT
      DO 100 I=1,13
  100 PHIWRK(I)=F(I)
      F(I)=-F(I)
C
C     FIND THE APPROXIMATE VALUE OF ZERO
C
      CALL ENSN(BGM,APZRO,AEIGN)
      DO 200 I=1,8
      F(I)=F(I)-BGM(1,I)*PHI(1)
  200 CONTINUE
      BGM(1,1)=AEIGN
C
C     SOLVE THE MATRIX EQUATION
C
  450 CALL LDLT(BGM,13,8,APZRO)
      CALL SLV(BGM,F,13,8)
C
C     FORM THE "PHI" AND "F" VECTORS
C
      PHIWRK(1)=-AEIGN*F(1)
      DO 500 I=2,13
  500 PHI(I)=F(I)
      TOTLAS=TOT(III)
      TOT(III)=PHIWRK(1)-HAVG(1)-HAVG(3)*(PHI(3)-TSAT)-(HAVG(6)+HCAVG)*(PHI(6)-T
     1SAT)-HAVG(5)*(PHI(5)-TSAT)-HAVG(12)*(PHI(12)-TSAT)
      CCNVER=CABS((TOT(III)-TOTLAS)/TOTLAS)
      RETURN
      END
```

62

```
      SUBROUTINE SQUARE
      IMPLICIT REAL*8(A-H,O-Z)
C
      COMMON /MTRX/ CORC(8,2),ENN(8,8),CCCL(8,2),AJ(2,2),AJI(2,2),
     1EAK(8,8),FE(8),BGM(13,8),COARD(13,2),F(13),FHI(13),
     2PHINRK(13),HAVG(13),TOT(101),AK,TINF,AP2RO,AEIGN,TSAT,HCAVG,CCNVER
      COMMON /FLP/ DTJ,AK,TINF,AP2RO,AEIGN,TSAT,HCAVG,CCNVER
      COMMON /IMTRX/ NCCN(2,8)
      DIMENSION GP(2),WF(2)
      DATA GP/.5773502691896300,-.5773502691896300/
      DATA WF/1.0D0,1.0C0/
C
      DO 300 I=1,2
      ZETA=GP(I)
      WX=WF(I)
      DO 300 J=1,2
      ETA=GP(J)
      WY=WF(J)
      WFACT=WX*WY
C
C     FORM THE ELEMENT PRODUCT MATRICES
C
100   CALL FORMH(ZETA,ETA)
200   DO 250 L=1,8
      DO 250 M=1,8
      EAK(L,M)=ENN(L,M)+WFACT*ENN(L,M)
250   CONTINUE
300   CONTINUE
350   DO 350 I=1,8
      DO 350 J=I,8
      ENN(I,J)=5.D-1*(ENN(I,J)+ENN(J,I))
      ENN(J,I)=ENN(I,J)
      RETURN
      SUBROUTINE FORMH(ZETA,ETA)
      IMPLICIT REAL*8(A-H,O-Z)
      COMMON /MTRX/ CORC(8,2),ENN(8,8),CCCL(8,2),AJ(2,2),AJI(2,2),
     1EAK(8,8),FE(8),BGM(13,8),COARD(13,2),F(13),FHI(13),
     2PHINRK(13),HAVG(13),TOT(101),AK,TINF,AP2RO,AEIGN,TSAT,HCAVG,CCNVER
      COMMON /FLP/ DTJ,AK,TINF,AP2RO,AEIGN,TSAT,HCAVG,CCNVER
      COMMON /IMTRX/ NCCN(2,8)
C
C     FORM THE SHAPE FUNCTION PARTIAL DERIVATIVES WITH RESPECT TO
C     GLOEAL COORDINATES
C
      CALL SHAPE(ZETA,ETA)
      CALL JACOB(AJ,DCCL,CORC,AJI,DTJ)
      DO 500 I=1,8
```

```
      CNZ=DCCL(I,1)
      CNY=DCOL(I,2)
      DCCL(I,1)=AJI(1,1)*DNZ+AJI(1,2)*CNY
      DCCL(I,2)=AJI(2,1)*CNZ+AJI(2,2)*CNY
  500
C
C     PFCCUCTS OF THE DERIVATIVES WITH RESPECT TC Z
C
      CC 700 I=1,8
      EEZ=CCOL(I,1)*DTJ
  700 ENN(I,J)=BZ*AK*DCCL(J,1)
C
C     PFCCUCTS OF THE DERIVATIVES WITH RESPECT TC Y
C
      CC 800 I=1,8
      BY=CCOL(I,2)*DTJ
      EOO J=1,8
  800 ENN(I,J)=BY*AK*DCOL(J,2)+ENN(I,J)
      RETURN
      SLEROUTINE SHAPE(ZETA,ETA)
      INFLICIT REAL*8(A-F,O-Z)
      CCCMCN /MTRX/ CORC(8,2),ENN(8,8),CCOL(8,2),AJ(2,2),AJI(2,2),
     1ENNW(8,8),FE(8),BGM(13,8),CQARD(13,2),F(13),FHI(13),
     2CCIHARK(13),FAVG(13),TOT(10),
      CCMMON /FLP/ DTJ,AK,TINF,APZRC,AEIGN,TSAT,FCAVG,CCNVER
      CCMMON /IMTRX/ NCCN(2,8)
      CIMENSICN CORDZ(4),CCRCY(4)
      CATA CORDZ/1.0D0,-1.0C0,-1.0C0,1.0C0/
      CATA CORDY/1.0D0,1.0D0,-1.0D0,-1.0C0/
C
      DFCS(ZETA,ETA,ZI,YI)=(1.0D0+ETA*YI)*ZI*(2.0C0*ZETA*ZI+ETA*YI)/4.D0
      DFCNZ(ZETA,ETA,YI)=-ZETA*(1.0D0+ETA*YI)
      DFCMY(ZETA,YI)=YI*(1.0C0-ZETA**2)/2.0D0
C
C     CLACRATIC ELEMENT FUNCTIONS
C
C
C     CCRNER NODES (1,3,5,7)
C
      IZ=0
   20 IZ=200 ICOL=1,7,2
      IZ=IZ+1
      YI=CORCY(IZ)
      ZI=CORCZ(IZ)
      CCCL(ICCL,1)=DFQS(ZETA,ZI,YI)
  200 DCCL(ICCL,2)=DFQS(ETA,ZETA,YI,ZI)
```

```
C
C     MID-SIDE NODES: 2,4
C                     6,8
C
      IN=0
      DO 250 IC2=2,6,4
      IC4=IC2+2
      IN=IN+2
      Z1=CORDZ(IN)
      Y1=CORDY(IN)
      CORDL(IC2,1)=DFQMZ(ZETA,ETA,Y1)
      CORDL(IC2,2)=DFQMY(ZETA,ETA,Y1)
      CORDL(IC4,1)=DFQMY(ZETA,ETA,Z1)
      CORDL(IC4,2)=DFQMZ(ETA,ZETA,Z1)
250   RETURN
      END
      SUBROUTINE JACOB(AJ,CCDL,CORD,AJI,CTJ)
C
C THIS SUBROUTINE WILL FORM THE JACOBIAN AND COMPUTE ITS DETERMINANT
C AND INVERSE
C         AJ= 2X2 JACOBIAN MATRIX
C         AJI= 2X2 INVERSE OF THE JACOBIAN
C         CTJ= DETERMINANT OF THE JACOBIAN
C         CORD= 8X2 MATRIX OF GLOBAL COORDINATES
C         DCOL= 8X2 MATRIX OF PARTIAL DERIVATIVES WITH RESPECT TO
C               LOCAL COORDINATES
C
      IMPLICIT REAL*8(A-H,O-Z)
      DIMENSION AJ(2,2),AJI(2,2),CCOL(8,2),CORD(8,2)
C
C FORM THE JACOBIAN
C
      DO 500 I=1,2
      DO 500 J=1,2
      AJ(I,J)=0.0D0
      DO 500 K=1,8
500   AJ(I,J)=AJ(I,J)+DCOL(K,I)*CORD(K,J)
C
C COMPUTE THE DETERMINANT
C
      CTJ=AJ(1,1)*AJ(2,2)-AJ(1,2)*AJ(2,1)
C
C COMPUTE THE INVERSE
C
      AJI(1,1)=AJ(2,2)/DTJ
      AJI(1,2)=-AJ(1,2)/CTJ
      AJI(2,1)=-AJ(2,1)/DTJ
      AJI(2,2)=AJ(1,1)/DTJ
```

```
      RETURN
      END
      SUBROUTINE ENSN(A,APZRO,ABIGN)                                    LDS0010
      IMPLICIT REAL*8(A-H,O-Z)
      DIMENSION A(13,8)
      ANE=0.0D0
  100 I=1,13
      ANE=ANE+DABS(A(I,1))
      APZRO=ANB*1.0D-15/DFLOAT(13)
      ABIGN=APZRO*1.0D30
      RETURN
      END
      SUBROUTINE LDLT(A,N,ASN)
C*****************************************************************       LDS0015
C*    A IS THE NAME OF THE COEFFICIENT MATRIX                    *       LDS0030
C*                                                               *       LDS0040
C*    N IS THE HALF BAND WIDTH OF THE SYSTEM                     *       LDS0050
C*    ASN IS THE CALCLLATEC VALUE CF ZERO                        *       LDS0060
C*                                                               *       LDS0070
C*    THIS SUBROUTINE DECOMPOSES THE COEFFICIENT MATRIX A*       *       LDS0080
C*    OF A SYMMETRICAL SYSTEM (A*)(X)=(B) INTC THE PRODLCT       *       LDS0090
C*    OF THE UPPER BAND ONLY IS USED AND IT MUST BE STCRED       *       LDS0100
C*    ARRAY (A) IS DESTROYED IN THE PRCCESS ANC THE REST         *       LDS0110
C*    THE SAME ARRAY. MATRIX (D) IS PUT IN THE FIRST CCLUMN      *       LDS0120
C*    CF THE MATRIX CONTAINS THE ELEMENTS CF THE UNIT TRIANGLLAR *       LDS0130
C*    IN BANDED FORM WITHOUT ITS IMPLIED UNIT DIAGCNAL ELEMENTS. *       LDS0140
C*                                                               *       LDS0150
C*    CODEC BY GILLES CANTIN, NAVAL POSTGRADUATE SCHOOL, MAY 1972 *      LDS0160
C*****************************************************************       LDS0170
      IMPLICIT REAL*8(A-H,O-Z)                                          LDS0180
      DIMENSICN A(13,8)
      AVSN=ASN*ASN
  100 I=1,NM
      DIAG=A(I,1)
  100 J=2,M
      IF(DABS(A(I,J)).LE.AVSN) A(I,J)=0.0D0
  300 J=2,N
      L=I+J-1
      IF(L.GT.N) GO TO 300
      IF(DABS(A(I,J)).LE.AVSN) GO TO 300
      AA=A(I,J)/DIAG
      K=J,M
      ML=I+K-J
  200 A(L,ML)=A(L,ML)-AA*A(I,K)
```

```
  300 CONTINUE
      RETURN
      END
      SUBROUTINE SLV(Z,B,N,M)
      IMPLICIT REAL*8 (A-H,O-Z)
C***********************************************************
C*   THIS SUBROUTINE PERFORMS A FORWARD SUBSTITUTION FOLLOWED BY A     *
C*   BACKWARD SUBSTITUTION FOR THE SYSTEM (A*)(X)=(B) AFTER THE        *
C*   MATRIX (A) HAS BEEN DECOMPOSED BY THE SUBROUTINE LDLT.           *
C*   A    IS THE NAME OF THE DECOMPOSED MATRIX OF COEFFICIENTS        *
C*   B    IS THE NAME OF THE COLUMN LOAD VECTOR OR RIGHT HAND MEMBER  *
C*        THE ANSWERS ARE RETURNED IN THIS VECTOR UPON EXIT          *
C*   N    IS THE NUMBER OF EQUATIONS IN THE SYSTEM                   *
C*   M    IS THE HALF BAND WIDTH OF THE SYSTEM                       *
C*                                                                   *
C*   AFTER ONE CALL TO LDLT, ONE CALL OF SLV PER LOAD VECTOR IS REQUIRED *
C*                                                                   *
C*   CODED BY GILLES CANTIN, NAVAL POSTGRADUATE SCHOOL, MAY 1972     *
C***********************************************************
      DIMENSION Z(13,8),B(13)
      NM=N-1
      DO 400 I=1,NM
      BI=B(I)
      DO 400 J=2,M
      L=I+J-1
      IF(L.GT.N) GO TO 400
      B(L)=B(L)-Z(I,J)*BI
  400 CONTINUE
      DO 500 I=1,N
      B(I)=B(I)/Z(I,1)
  500 CONTINUE
      DO 600 L=2,N
      IR=N-L+1
      BIFF=B(IR+1)
      DO 600 J=2,M
      IRQ=IR-J+2
      IF(IRQ.LE.0) GO TO 600
      B(IRQ)=B(IRQ)-Z(IRQ,J)*BIFF
  600 CONTINUE
      RETURN
      END
```

LDS00230
LDS00240
LDS00250
LDS00260
LDS00270
LDS00280
LDS00290
LDS00300
LDS00310
LDS00320
LDS00330
LDS00340
LDS00350
LDS00360
LDS00370
LDS00380
LDS00390
LDS00400
LDS00410
LDS00420

67

BIBLIOGRAPHY

1. Tien, C.L., "Fluid Mechanics of Heat Pipes," _Annual Review of Fluid Mechanics_, v. 7, p. 174, 1975.

2. Ballback, L.J., _The Operation of a Rotating, Wickless Heat Pipe_, M.S. Thesis, Naval Postgraduate School, Monterey, California, December 1969.

3. Daley, T.J., _The Experimental Design and Operation of a Rotating, Wickless Heat Pipe_, M.S. Thesis, Naval Postgraduate School, Monterey, California, June 1970.

4. Daniels, T.C., Al-Jumaily, F.K., _Theoretical and Experimental Analysis of a Rotating, Wickless Heat Pipe_, Proceedings of the 1st International Heat Pipe Conference, Stuttgart, 1973.

5. Daniels, T.C., Al-Jumaily, F.K., "Investigations of the Factors Affecting the Performance of a Rotating Heat Pipe," _International Journal of Heat and Mass Transfer_, v. 18, p. 961, 1975.

6. Marto, P.J., _Performance Characteristics of Rotating, Wickless Heat Pipes_, Proceedings of the 2nd International Heat Pipe Conference, p. 281-291, Bologna, 1976.

7. Newton, W.H., _Performance Characteristics of Rotating, Non-Capillary Heat Pipes_, M.S. Thesis, Naval Postgraduate School, Monterey, California, June 1971.

8. Schafer, C.E., _Augmenting the Heat Transfer Performance of Rotating, Two-Phase Thermosyphons_, M.S. Thesis, Naval Postgraduate School, Monterey, California, December 1972.

9. Woodard, J.S., _The Operation of Rotating, Non-Capillary Heat Pipes_, M.S. Thesis, Naval Postgraduate School, Monterey, California, March 1972.

10. Sparrow, E.M., Gregg, J.L., "A Theory of Rotating Condensation," _Journal of Heat Transfer_, v. 81, p. 113-120, May 1959.

11. Myers, G.E., _Analytical Methods in Conduction Heat Transfer_, p. 383-387, McGraw-Hill, 1971.

12. Lew, G.T., _A Three-Dimensional Solution of the Transient Field Problem Using Isoparametric Finite Elements_, M.S. Thesis, Naval Postgraduate School, Monterey, California, December 1972.

13.   Arpaci, V.S., <u>Conduction Heat Transfer</u>, p. 44-58, Addison-Wesley, 1966.

14.   Zienkiewicz, O.C., <u>The Finite Element Method in Structural and Continuum Mechanics</u>, McGraw-Hill, 1967.

15.   Zienkiewicz, O.C., Parekh, C.J., "Transient Field Problems: Two-Dimensional and Three-Dimensional Analysis by Isoparametric Finite Elements," <u>International Journal for Numerical Methods in Engineering</u>, v. 2, No. 1, p. 61-71, January-March 1970.

16.   Kern, D.O., Kraus, A.D., <u>Extended Surface Heat Transfer</u>, p. 91-101, McGraw-Hill, 1972.

INITIAL DISTRIBUTION LIST

|		No. Copies
1.	Defense Documentation Center Cameron Station Alexandria, Virginia 22314	2
2.	Library, Code 0212 Naval Postgraduate School Monterey, California 93940	2
3.	Mechanical Engineering Department Naval Postgraduate School Monterey, California 93940	1
4.	Assoc. Professor P. J. Marto (thesis advisor) Department of Mechanical Engineering Naval Postgraduate School Monterey, California 93940	1
5.	Ens. Robert D. Corley 1921 Nottingham Blvd. Fort Worth, Texas 76112	1